

1 **Do Land Models Miss Key Soil Hydrological Processes Controlling Soil Moisture Memory?**

2  
3 **Mohammad A. Farmani<sup>1</sup>, Ali Behrangi<sup>1,2</sup>, Aniket Gupta<sup>1</sup>, Ahmad Tavakoly<sup>3,4</sup>, Matthew**  
4 **Geheran<sup>3</sup>, and Guo-Yue Niu<sup>1</sup>**

5  
6  
7 <sup>1</sup>Department of Hydrology and Atmospheric Sciences, University of Arizona, Tucson, AZ, USA,

8 <sup>2</sup>Department of Geosciences, University of Arizona, Tucson, AZ, USA,

9 <sup>3</sup>US Army Engineer Research and Development Center, Coastal and Hydraulics Laboratory,  
10 Vicksburg, MS, USA,

11 <sup>4</sup>Earth System Science Interdisciplinary Center, University of Maryland, College Park, MD,  
12 USA

13  
14  
15  
16  
17 Corresponding author: Mohammad Farmani, email: [farmani@arizona.edu](mailto:farmani@arizona.edu)

18 Guo-Yue Niu, email: [niug@arizona.edu](mailto:niug@arizona.edu)

19  
20  
21  
22  
23  
24  
25  
26  
27  
28  
29  
30  
31  
32  
33  
34  
35  
36  
37  
38  
39 **Key Points:**

40 Van-Genuchten soil hydraulics improves long-term Soil Moisture Memory (SMM) of the  
41 topsoil.

42 Surface ponding enhances soil moisture memory in both topsoil and the root zone.

43 Representing preferential flow improves both short-term and long-term SMM in both the  
44 topsoil and root zone.

45       **Abstract**

46  
47       Soil moisture memory (SMM), which refers to how long a perturbation in Soil Moisture (SM) can  
48       last, is critical for understanding climatic, hydrologic, and ecosystem interactions. Most land  
49       surface models (LSMs) tend to overestimate surface soil moisture and its persistency (or SMM),  
50       sustaining spuriously large soil surface evaporation during dry-down periods. We attempt to  
51       answer a question: Do LSMs miss or misrepresent key hydrological processes controlling SMM?  
52       We use a version of Noah-MP with advanced hydrology that explicitly represents preferential flow  
53       and surface ponding and provides optional schemes of soil hydraulics. We test the effects of these  
54       processes that are generally missed by most LSMs on SMM. We compare SMMs computed from  
55       various Noah-MP configurations against that derived from the Soil Moisture Active Passive  
56       (SMAP) Level 3 soil moisture and in-situ measurements from the International Soil Moisture  
57       Network (ISMN) from year 2015 to 2019 over the contiguous United States (CONUS). The results  
58       suggest that 1) soil hydraulics plays a dominant role, and the Van-Genuchten hydraulic scheme  
59       reduces the overestimation of the long-term surface SMM produced by the Brooks-Corey scheme,  
60       which is commonly used in LSMs; 2) explicitly representing surface ponding enhances SMM for  
61       both the surface layer and the root zone; and 3) representing preferential flow improves the overall  
62       representation of soil moisture dynamics. The combination of these missing schemes can  
63       significantly improve the long-term memory overestimation and short-term memory  
64       underestimation issues in LSMs. We suggest that LSMs for use in seasonal-to-subseasonal climate  
65       prediction should, at least, adopt the Van-Genuchten hydraulic scheme.

66  
67  
68  
69  
70  
71  
72  
73  
74  
75  
76  
77  
78  
79  
80  
81  
82  
83  
84  
85  
86  
87  
88  
89  
90  
91  
92  
93

94 **Plain Language Summary**

95

96 Land surface models (LSMs) represent the physical and bio-geochemical exchanges of mass and  
97 energy between surface and atmosphere. Such exchanges are extensively dependent on the surface  
98 soil water amount and its persistence. This study explores key hydrological processes that may be  
99 missed by LSMs but important for weather and climate predictions. Through virtual experiments  
100 with a state-of-the-art model, we found that soil hydraulics (representing how efficiently soil can  
101 hold/release water under varying pressure) is particularly effective in sustaining soil moisture.  
102 Additionally, we found that allowing water to pond on the soil surface helps improve the model's  
103 soil moisture persistency. Furthermore, enhanced soil permeability due to soil macropores also  
104 regulates the water movement hence improving the soil moisture persistency. Overall, future  
105 LSMs should refine the treatment of soil water retention capability and consider the effects of soil  
106 macropores and surface ponding to improve weather and seasonal climate predictions.

107

## 108 1. Introduction

109

110 Land surface models' (LSMs) efficacy in simulating climate feedback mechanisms critically  
111 depends on the soil water retention capacity and soil moisture persistency. Rainwater that rapidly  
112 infiltrates into deeper subsoil strata is unavailable to be returned to the atmosphere through  
113 evaporation, thereby preventing potential atmospheric feedback loops (McColl et al., 2019). The  
114 influence of soil moisture on climate predictions at seasonal-to-sub-seasonal (S2S) scales is well-  
115 recognized due to its role in the exchange of surface energy and water fluxes with the atmosphere  
116 (Koster et al., 2002; Randal D. Koster et al., 2009; Koster et al., 2010; Koster & Suarez, 2001).  
117 Water stored in soil and aquifers, which variably persists from seasons to years, is known to affect  
118 precipitation variability (Koster & Suarez, 1999, 2001). This impact is particularly pronounced in  
119 regions transitioning from dry to wet conditions, where evapotranspiration (ET) is highly sensitive  
120 to soil moisture levels (Zhichang Guo et al., 2006; Koster et al., 2004; Koster & Suarez, 2001;  
121 Seneviratne, Koster, et al., 2006). While the nature and scale of soil moisture-precipitation  
122 feedback are still being debated (Findell et al., 2011; Taylor et al., 2013), numerous studies have  
123 emphasized the importance of soil moisture initialization and its persistency for accurate climate  
124 predictions (Dirmeyer, 2011; Mei & Wang, 2012; Shellito et al., 2016; Tuttle & Salvucci, 2016;  
125 Hossein Yousefi Sohi et al., 2024; Zebarjadian et al., 2024; Zeng et al., 2010). The degree of soil  
126 moisture-precipitation coupling widely varies across different climate models (Koster et al., 2004;  
127 Koster & Suarez, 1999; Moghisi et al., 2024; Seneviratne & Koster, 2012; Taylor et al., 2013), and  
128 discrepancies in the modeled soil moisture by LSMs for climate modeling are notable (Boone,  
129 2004; Souri et al., 2024).

130

131 Refinement of soil moisture-precipitation feedback in LSMs is hindered by the lack of large-scale  
132 observational data, challenging the improvement and validation of model simulations (Koster et  
133 al., 2010; Koster & P. Mahanama, 2012; Koster & Suarez, 1999, 2001; Seneviratne & Koster,  
134 2012). This shortfall highlights the necessity for more detailed representations of land-atmosphere  
135 feedback mechanisms that are crucial for extreme weather event predictions, yet are typically  
136 parameterized rather than explicitly resolved in models (McColl et al., 2019; Pastorello et al.,  
137 2020). Integrating extensive observational data is vital for simulating the intricacies of climate and  
138 weather and improving model predictive skill (Koster et al., 2017; R. D. Koster et al., 2009;  
139 McColl et al., 2019; Shellito et al., 2018). Recent advancements in remote sensing observations  
140 have enabled analyses of interactions between near-surface soil and the atmosphere. Nonetheless,  
141 the paucity of root zone data complicates the investigation of deep soil dynamics. Numerous  
142 studies have utilized satellite soil moisture products to evaluate and refine models, focusing on the  
143 spatial and temporal patterns of soil moisture variability (Randal D. Koster et al., 2009; Yang et  
144 al., 2020). In particular, the Soil Moisture Active Passive (SMAP) mission has been extensively  
145 employed to assess model performance (McColl, Alemohammad, et al., 2017; McColl et al., 2019;  
146 McColl, Wang, et al., 2017; Shellito et al., 2016; Shellito et al., 2018).

147

148 The concept of Soil Moisture Memory (SMM)—the duration required for a perturbation, such as  
149 rainfall, to dissipate—becomes essential for understanding the land-atmosphere interactions.  
150 SMM encapsulates the temporal variations of soil moisture, reflecting the exchange of fluxes  
151 between land and atmosphere. Therefore, SMM is an important metric for evaluating LSMs, since  
152 one of their functions is to provide surface flux exchanges and boundary conditions for  
153 atmospheric models (Z. Guo et al., 2006; Koster et al., 2004; Randal D. Koster et al., 2009; R. D.

154 Koster et al., 2009; Seneviratne, Koster, et al., 2006). SMM also facilitates the comparison of how  
155 quickly soil loses water between observations and various models, providing insights into the  
156 mechanisms within LSMs and their hydrometeorological responses. Moreover, analyzing SMM  
157 can yield valuable data on the configurations and hydrological parameterizations of specific LSMs,  
158 thus improving our understanding of how different configurations impact model performance,  
159 particularly in soil moisture representation. For instance, Shellito et al. (2018) measured the drying  
160 rate of surface soil moisture, which they considered as soil moisture memory, using SMAP data  
161 and the Noah LSM during the initial 1.8 years following SMAP's launch. They concluded that  
162 Noah shows a slower drying rate and a longer surface SMM compared with SMAP, due likely to  
163 the too strong soil water suction represented by Noah.

164  
165 Determining SMM is not straightforward due to the variety of calculation methods proposed by  
166 researchers (Ghannam et al., 2016; Katul et al., 2007; Koster et al., 2004; Koster et al., 2002;  
167 Randal D. Koster et al., 2009; Koster & Suarez, 1999, 2001; Mao et al., 2020; McColl,  
168 Alemohammad, et al., 2017; McColl et al., 2019; McColl, Wang, et al., 2017; Seneviratne, Koster,  
169 et al., 2006; Shellito et al., 2016), each introducing its own level of uncertainty. Traditionally, soil  
170 moisture has been conceptualized as a red noise process, forming the basis for SMM calculations  
171 (T. L. Delworth & Manabe, 1988). This approach has led to the definition of SMM as the e-folding  
172 autocorrelation timescale within such a process (Delworth & Manabe, 1989). SMM has also been  
173 characterized using various other autocorrelation-based methods, such as the integral timescale  
174 (Ghannam et al., 2016; Nakai et al., 2014), soil moisture variance spectrum (Katul et al., 2007;  
175 Nakai et al., 2014), and the constant time lag autocorrelation (Koster & Suarez, 2001; Seneviratne,  
176 Lüthi, et al., 2006). Traditionally, these models were applied to monthly datasets. However, this  
177 approach risks overlooking dynamic processes governed by limitations in water and energy  
178 (Mccoll et al., 2019). Consequently, there has been a shift away from their use towards recent high-  
179 resolution observational and modeling data. Therefore, there is a need for further research to refine  
180 SMM measurement that can then be used as a benchmark for assessing LSMs (Mccoll et al., 2019).

181  
182 McColl et al. (2019) categorized soil water loss into two main categories: water-limited (long-  
183 term) and energy-limited (short-term). The energy-limited regime is a process where water loss is  
184 constrained by available energy and lasts from hours to a few days. In contrast, the water-limited  
185 regime is a process where water loss depends on the available water and spans longer periods, such  
186 as weeks, months, and seasons. McColl et al. (2019) specified that ET and drainage are the main  
187 controllers of long-term and short-term memories, respectively. Utilizing a two-year dataset from  
188 the SMAP mission and simulations from the Goddard Earth Observing System Model, Version 5  
189 (GEOS-5), McColl et al. (2019) conducted a global analysis under various climatic and land  
190 conditions. Their analysis revealed that GEOS-5 tends to overpredict the duration of water-limited  
191 memory and underpredicts energy-limited memory compared to SMM inferred from SMAP data,  
192 while the results were not affected by the SMAP sampling frequency of 3 days. Building on this,  
193 He et al. (2023) employed the hybrid memory approach proposed by McColl et al. (2019) to assess  
194 the hydrometeorological response of various LSMs, including GLDAS-CLSM, GLDAS-Noah,  
195 MERRA2, NCEP, ERA5, and JRA55, against SMAP observations for 2015 – 2020. The authors  
196 observed that LSMs generally overestimate memory in water-limited regime and significantly  
197 underestimate it in energy-limited regime. Moreover, their study suggested that discrepancies in  
198 SMM representation within LSMs are more attributable to the physical processes incorporated

199 rather than factors such as soil layer thickness or the nature of model simulations (online/offline)  
200 (He et al., 2023).

201  
202 A recent review on SMM identified the soil properties and processes as an important controlling  
203 factor of SMM in addition to atmospheric forcings and land use and management for future studies  
204 to examine the fundamental mechanisms of SMM emergence (Rahmati et al., 2024). Based on the  
205 works of McColl et al. (2019) and He et al. (2023), this study aims to examine the impacts of key  
206 soil hydrological processes and soil hydraulics on SMM that may be missed in most LSMs. Current  
207 LSMs may be not enough to address the uncertainties of SMM estimates for incomplete  
208 representations of key hydrological processes controlling SMM and uncertainties in soil hydraulic  
209 parameters (Rahmati et al., 2024). As such, we use a version of Noah-MP with advanced  
210 hydrological representations of preferential flow, surface ponding, runoff of surface ponded water  
211 (infiltration excess runoff), and lateral infiltration, etc. (Niu et al., 2024). We conduct model  
212 experiments with various soil hydraulic parametrizations of those by Brooks and Corey (1964) and  
213 Van-Genuchten (1980), preferential flow, and surface ponding depth. Our analysis investigates  
214 the impact of these configurations on soil moisture persistency across ET regimes and drainage,  
215 so that it can provide insight into these missing physical processes affecting SMM. By comparing  
216 SMM produced by various settings of Noah-MP with SMAP Level 3 data and ISMN observations  
217 from 2015 to 2019 over the CONUS, we seek to identify key processes and soil hydraulic schemes  
218 controlling SMM and thus provide guidance for future developments of LSMs (e.g., reduce the  
219 prevalent SMM overestimations in LSMs).

220

## 221 **2. Materials and Methods**

222

223 SMM denotes the duration required for a perturbation to dissipate, or the period from the start to  
224 the end of a perturbation. For instance, following precipitation, the change in near-surface soil  
225 moisture marks the beginning of the perturbation. This excess moisture gradually diminishes due  
226 to flux exchange or percolation to deeper soil layers. The moisture level of soil plays a critical  
227 role in influencing water loss patterns. Following rainfall, the upper layer of soil initially holds  
228 more moisture than its field capacity ( $\theta_{fc}$ ), causing runoff and drainage (see Figure 1a).  
229 Subsequently, as the soil gradually dries, its moisture content reduces to a range between  $\theta_{fc}$  and  
230 the critical threshold ( $\theta_c$ ). This phase leads to consistent water loss at the maximum ET rate, known  
231 as Stage-I ET. As this process continues, the soil moisture falls below  $\theta_c$  (Figure 1a), at which  
232 stage ET becomes limited by the available water, termed Stage-II ET or ET at water-limited regime  
233 (illustrated in Figure 1a & b). Ultimately, when the soil moisture drops below the wilting point  
234 ( $\theta_w$ ), water no longer leaves the soil. Therefore, the whole process of water loss depends on the  
235 soil's moisture level and falls into two main types: energy-limited including unresolved drainage,  
236 and Stage-I ET, and water-limited including Stage-II ET (Figure 1b) (Mccoll et al., 2019; He et al.  
237 2023). Energy-limited, green strips, and water-limited regimes, dotted-lines, are shown in soil  
238 moisture times series at the Tonzi Ranch station (Figure 1c).

239

240

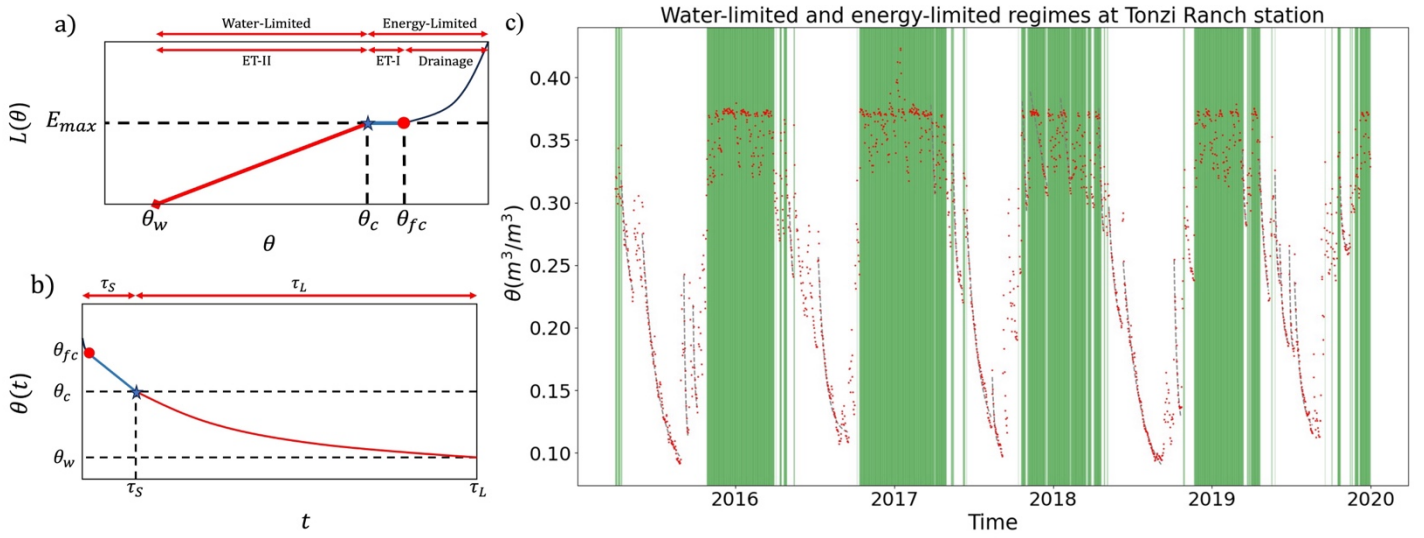


Figure 1 Schematic diagrams of (a) surface water loss process and (b) soil moisture memory at different soil moisture regimes [adapted from (McColl, Wang, et al., 2017b)]. Note that the x-axis in (a) refers to soil moisture ( $\text{m}^3\text{m}^{-3}$ ), and y-axis refers to surface water loss rate,  $L(\theta)$  (mm/s);  $E_{\max}$  is the maximum evaporation rate (mm/s). In (b), x-axis refers to time (e.g., days) and y-axis to SM content ( $\text{m}^3\text{m}^{-3}$ ). Panel (c) shows the SM time series for the Tonzi Ranch station, with green periods indicating energy-limited regime and dotted lines representing water-limited regime.  $\theta_w$ ,  $\theta_c$  and  $\theta_{fc}$  refer to the wilting point, critical point, and field capacity, respectively.

241  
242

## 243 2.1. Soil Moisture Memory of Water-Limited Regime ( $\tau_L$ ) and Energy-Limited 244 Regime ( $\tau_S$ )

245

246 McColl et al. (2019) considered the SMM concept as it relates to two regimes: a) the memory of  
247 water-limited regime ( $\tau_L$ ), specified by 'L' abbreviation of Long-term, b) the memory of energy-  
248 limited regime ( $\tau_S$ ), specified by 'S' abbreviation of Short-term. Their model incorporates a  
249 deterministic equation to represent water-limited processes during soil moisture drydown periods.  
250 However, energy-limited processes occur over shorter timescales and present a challenge for  
251 current satellite technologies to provide precise observations. McColl et al. (2019) highlighted that  
252 drainage is not a completely resolved process by satellite observations. To address this gap,  
253 McColl et al. (2019) proposed a stochastic equation to capture the unresolved nature of energy-  
254 limited processes.

255

256 The hybrid model is formulated by McColl et al. (2019) as follows:

$$\frac{d\theta(t)}{dt} = \begin{cases} \frac{-\theta(t) - \theta_w}{\tau_L}, P = 0 \\ \frac{-\theta(t) - \bar{\theta}}{\tau_S} + \varepsilon(t), P > 0 \end{cases} \quad (1)$$

257 where,  $\theta$  is the volumetric soil moisture,  $P$  indicates precipitation,  $\theta_w$  is the minimum soil moisture,  
 258  $\bar{\theta}$  is the time-averaged SM, and  $\varepsilon(t)$  is a random variable with a mean of zero.  $\tau_L$  and  $\tau_S$  are SMM  
 259 for the water-limited and energy-limited regimes, respectively. McColl et al. (2019) solved these  
 260 equations, demonstrating that the memories can be expressed as:

$$\theta(t) = \Delta\theta \exp\left(\frac{-t}{\tau_L}\right) + \theta_w P = 0 \quad (2)$$

$$\tau_S = \frac{-\frac{\Delta t}{2}}{\log} \quad (3)$$

261  $\Delta\theta$  represents the soil moisture changes during drydown,  $\Delta t$  is the temporal resolution of the soil  
 262 moisture data,  $\alpha$  is the precipitation intensity,  $\Delta z$  is soil layer thickness, and  $\overline{\Delta\theta_+} = \theta(t) - \theta(t - \Delta t)$   
 263 represents a positive increment in soil moisture. (McColl, Alemohammad, et al., 2017) defined  
 264  $\frac{\Delta z [\overline{\Delta\theta_+}]}{\alpha}$  as stored fraction of precipitation, indicating the average proportion of water that still exists  
 265 in soil layer  $\Delta t$  days after rainfall. McColl et al. (2019) declared that the short-term memory in  
 266 their hybrid model is dominated by drainage when the sampling is relatively high (as in the case  
 267 of SMAP's sampling frequency of 3 days). This approach and its rationale are further elaborated  
 268 in (McColl, Alemohammad, et al., 2017) and McColl et al. (2019).  
 269

270  
 271 In the analysis of water-limited memory, we fitted Equation 2 to the soil moisture time series  
 272 during specific drydown intervals. Then,  $\tau_L$  was extracted as a parameter from the fitting curve  
 273 (black dotted lines in Figure 1c). In contrast, short-term memory was determined directly using  
 274 Equation 3, as indicated by the green periods in Figure 1c. Further information about the criteria  
 275 for calculating memories can be found in McColl et al. (2019).  
 276

## 277 **2.2. Description of Datasets**

278  
 279 We use high-resolution atmospheric forcing datasets to drive the Noah-MP LSM. This model is  
 280 set up to simulate soil moisture dynamics, featuring advanced infiltration and water retention  
 281 processes. Additionally, it includes a precise parameterization for ponding depth. This setup  
 282 facilitated five distinct experiments. Then, we used surface and root zone soil moisture data derived  
 283 from the Noah-MP experiments, SMAP Level 3 surface soil moisture measurements, and root zone  
 284 soil moisture measurements from the International Soil Moisture Network (ISMN) to calculate the  
 285 hybrid SMM. The rest of this section describes in detail the forcing and observational datasets, the  
 286 Noah-MP LSM configurations, the employed infiltration and water retention schemes, and the  
 287 ponding depth threshold criterion.  
 288  
 289

### 290 **2.2.1 Atmospheric Forcing, Soil and Vegetation Parameters**

291



292 For modeling purposes, this study utilized the North American Data Assimilation System Phase 2  
293 (NLDAS-2) near-surface meteorological data at an hourly interval and 0.125° spatial resolution.  
294 This dataset encompasses a range of variables including air temperature, specific humidity, wind  
295 speed, surface pressure, shortwave and longwave radiation, and precipitation (Xia et al., 2012).  
296 We also used precipitation data from the Integrated Multi-satellite Retrievals for Global  
297 Precipitation Measurement (IMERG-Final) dataset (Huffman et al., 2020; Jawad et al., 2024; H.  
298 Yousefi Sohi et al., 2024), which offers half-hourly measurements across a 0.1° grid extending  
299 from 60°S to 60°N. Subsequently, the IMERG-Final data were mapped to the 0.125° resolution of  
300 NLDAS-2 using bilinear interpolation. These precipitation data sources were integrated into the  
301 short-term SMM computation process. To integrate the IMERG precipitation product into the  
302 model, we modified the forcing component of the Noah-MP code. Specifically, an average of  
303 NLDAS-2 and IMERG precipitation was employed when NLDAS-2 reported negative  
304 precipitation values, which was particularly significant in coastal regions. This adjustment  
305 enhanced the accuracy of precipitation inputs, contributing to more reliable simulations in these  
306 areas.

307 To ascertain soil and vegetation parameters, the hybrid State Soil Geographic Database  
308 (STATSGO) with a 1-km resolution and the United States Geological Survey's (USGS) 24-  
309 category vegetation classification were employed. The datasets were aggregated to align with a  
310 0.125° resolution, which is consistent with the NLDAS-2 forcing data. This process included  
311 determining the dominant soil and vegetation types for each grid cell. Subsequently, the lookup  
312 tables within the Noah-MP model (Niu et al., 2020) were used to assign the relevant parameters to  
313 the corresponding soil and vegetation categories.

### 314 **2.2.2 SMAP L3 Surface Soil Moisture**

315  
316 Since its successful deployment on January 31, 2015, the Soil Moisture Active Passive (SMAP)  
317 observatory has consistently provided global volumetric soil moisture estimates every two or three  
318 days (Entekhabi et al., 2010). Its onboard radiometer, operating in the L-band frequency of the  
319 microwave spectrum, senses the top five centimeters of the soil column. In this study, we selected  
320 the SMAP Level 3 morning overpass due to the greater likelihood of air and surface temperature  
321 equilibrium during these hours, a critical condition for the SMAP retrieval algorithm. The L3  
322 SMAP data used here span from 2015 to 2020, have a spatial resolution of 9 kilometers and are  
323 instrumental in calculating SMM across the Continental United States (CONUS).

324  
325 In line with established methodologies from previous research (He et al., 2023; Mccoll et al.,  
326 2019), a quality control protocol was deemed necessary to refine soil moisture data in regions  
327 affected by dense vegetation, bodies of water, and permafrost, thereby mitigating noise present in  
328 satellite measurements (He et al., 2023; Mccoll et al., 2019; McColl, McColl, Wang, et al., 2017).  
329 However, this study is conducted to determine SMM to deepen our knowledge of physical  
330 processes and to get closer to optimal soil hydraulic parametrizations within Noah-MP. This is  
331 achieved through a comparative analysis of SMM derived from SMAP and Noah-MP datasets.  
332 Given that a specific parametrization within Noah-MP has a pronounced impact on the eastern  
333 region of the Continental United States (CONUS)—a region that also corresponds with a  
334 significant portion of SMAP's low-quality data—we chose not to filter SMAP data to fully capture  
335 the parametrization effects within our study's geographical focus. This approach was intended to  
336 maintain consistency across figures and enhance the presentation of our findings. Furthermore, our

337 objective is to showcase the physical process involved in SMM, rather than focusing on model  
338 accuracy in comparison with SMAP data. Note that the SMM maps from McColl et al (2019) and  
339 He et al (2023) demonstrated the effect of removing SMAP low-quality data, and hence we did  
340 not include the map of locations with high-quality SMAP data. Given that the surface water  
341 balance is sensitive to the temporal resolution of the analyzed surface soil moisture data, the SMAP  
342 L3 soil moisture data are resampled to achieve a consistent sampling frequency of one per three  
343 days at each pixel (He et al., 2023; McColl, Wang, et al., 2017).  
344

### 345 2.2.3 International Soil Moisture Network (ISMN)

346  
347 In evaluating the Noah-MP model's parametrization for the root zone soil moisture, SMM is  
348 computed using both the model's outputs and in situ observations across the CONUS. We obtained  
349 the in situ soil moisture data from the International Soil Moisture Network (ISMN) portal (Dorigo  
350 et al., 2011), which compiles quality-controlled measurements from various sensors across  
351 multiple networks, Figure 2. We exclude stations with less than 90% of their data rated as “good”  
352 quality. Despite the diversity of sensor types within ISMN, its stringent quality assurance protocols  
353 suggests that it is a reliable benchmark for validating soil moisture products (Colliander et al., 2017;  
354 Shellito et al., 2016). For the representation of root zone soil moisture, we select only the data from  
355 the top 1 meter of soil flagged as “good” quality. These measurements are averaged, i.e., hourly  
356 data aggregated to daily means, and the daily time series are used to compute both long-term and  
357 short-term SMM.

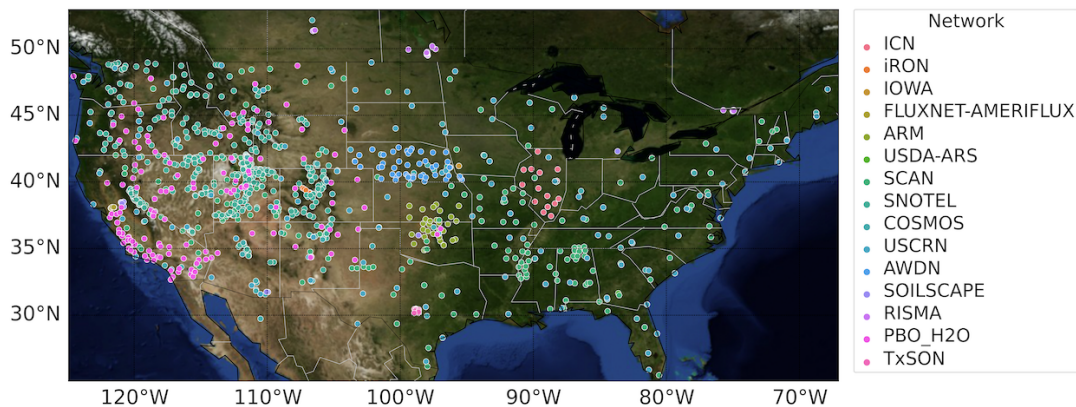


Figure 2 ISMN in-situ locations and networks over CONUS.

358

### 359 2.3 Noah-MP with Advanced Soil Hydrology

360  
361 In this study, we choose Noah-MP (Niu et al., 2024; Niu et al., 2011; Yang et al., 2011) for its  
362 extensive use within the Weather Research and Forecasting (WRF) model, the Unified Forecast  
363 System (UFS) for weather and short-term climate projections, and the National Water Model  
364 (NWM) for streamflow and water resource forecasting. The "semi-tile" sub-grid methodology of  
365 Noah-MP enables detailed calculation of surface energy and fluxes, differentiating effectively  
366 between bare and vegetated terrains to precisely compute variables such as latent and sensible heat  
367 fluxes (Agnihotri et al., 2023).

368  
369  
370  
371  
372  
373  
374  
375  
376  
377  
378  
379  
380

The Noah-MP version used in this study includes additional developments in plant hydraulics that explicitly represent plant water storage supplied by root water uptake driven by the hydraulic gradient between the soil and roots (Niu et al., 2020) and advanced soil hydrology that solves mixed-form Richards' equation and thus explicitly represents surface ponding, infiltration of surface ponded water, and preferential flow (Niu et al, 2024). As such, current Noah-MP accounts for water flow driven by the hydraulic gradients from the soil to the vegetation canopy to meet the plant transpiration demand. It also accounts for subgrid variability in infiltration capacity through a fractional area of preferential flow pathways caused by soil macropores in the fields. A detailed description of the underlying physical mechanisms for the schemes used in this study can be found in Niu et al, (2024), also a brief description of equations and parameters is included in supporting material.

381 **The Mixed-Form Richards' Equation:** Most LSMs solve the mass-based (or  $\theta$ -based) Richards'  
382 Equation (RE) for unsaturated soils(Chen & Dudhia, 2001; Oleson et al., 2010) and thus are not  
383 adequate to represent saturated conditions, e.g., surface ponding and groundwater dynamics. The  
384 current Noah-MP adopts the methodology of (Celia et al., 1990) to solve the mass-pressure ( $\theta$ -h)  
385 mixed-form RE (MF). The new solver solves pressure head,  $h$ , and conserves mass due to the mass  
386 ( $\theta$ ) constraint. To achieve a more accurate solution of  $h$  and mass balance, the solver takes an  
387 adaptive time stepping scheme.

388 Surface ponding occurs when the pressure head of the surface layer is greater than the air entry  
389 pressure, and the upper boundary condition (BC) shifts from flux BC to head BC following  
390 Paniconi (1994). Infiltration-excess runoff occurs when the surface ponding depth,  $H_{top}$ , surpasses  
391 a predefined threshold,  $H_{top,max}$ , at which the surface ponded water at local depressions of a model  
392 grid starts to be connected and runs off. The model extends its vertical domain to the bedrock depth  
393 (Pelletier et al., 2016) at which the lower BC is set up as a zero-flux BC. Groundwater discharge  
394 is simply represented using the TOPMODEL concept as a function of water table depth, which is  
395 determined by the modeled pressure head, which is interpolated between saturated zone and its  
396 overlying unsaturated zone.

397 **Optional Soil Hydraulics Schemes:** The current Noah-MP provides optional hydraulics schemes  
398 of the Van Genuchten-Mualem (VGM) and the Brooks-Corey with Clapp-Hornberger (BC/CH)  
399 parameters. To facilitate quicker convergence, particularly near saturation, we smoothed the  
400 BC/CH water retention curve using a polynomial function following (Bisht et al., 2018).

401 **Representing Preferential Flow:** To represent preferential flow, current Noah-MP adopts a dual-  
402 permeability model (DPM) approach, partitioning the model grid into two domains: one  
403 representing rapid flow with reduced suction head (macropores) and the other for slower matrix  
404 flow, following Šimůnek & van Genuchten, (2008) and Gerke and van Genuchten (1993a,b, 1996)  
405 (Gerke & van Genuchten, 1993a, 1993b; Gerke & van Genuchten, 1996; Šimůnek & Van  
406 Genuchten, 2008). This approach represents subgrid variability in infiltration capacity through a  
407 fractional area of soil macropores in the fields,  $F_a$ , (or volumetric fraction of macropores). DPM  
408 also represents water transfer between the two pore domains, which can be either be positive  
409 ("lateral infiltration" during rainy days) or negative (diffusion from micropores to drier  
410 macropores). It also accounts for lateral movement of surface ponded water from the matrix to  
411 macropore domains at the soil surface. The aggregated water content ( $\theta$ ) and vertical water flux

412 (q) for a grid cell are given by  $\theta = F_a \theta_a + (1-F_a) \theta_i$ , and  $q = F_a q_a + (1-F_a) q_i$ , respectively,  
 413 where  $q$  denotes a water flux and the subscripts a and i respectively indicate macropore and  
 414 micropore domains. This approach also extends to other water fluxes, such as direct evaporation  
 415 from soil surface,  $E_{soil}$ , and groundwater recharge.

416

417 Table 1 Noah-MP Options used in this study.

418

Process	Options	Schemes
Dynamic vegetation	DVEG = 2	Dynamic vegetation
Canopy stomatal resistance	OPT_CRS = 1	Ball-Berry type
Moisture factor for stomatal resistance	OPT_BTR = 1	Plant water stress
Runoff and groundwater	OPT_RUN = 1	TOPMODEL with groundwater
Surface layer exchange coefficient	OPT_SFC = 1	Monin-Obukhov similarity theory (MOST)
Radiation transfer	OPT_RAD = 1	Modified two-stream
Ground snow surface albedo	OPT_ALB = 3	Two-stream radiation scheme (Wang et al., 2022)
Precipitation partitioning	OPT_SNF = 5	Wet bulb temperature (Wang et al., 2019)
Lower boundary condition for soil temperature	OPT_TBOT = 2	2-m air temperature climatology at 8m
Snow/soil temperature time scheme	OPT_STC = 1	Semi-implicit
Surface evaporation resistance	OPT_RSF = 1	Sakaguchi and Zeng (2009)
Root profile	OPT_ROOT = 1	Dynamic root (Niu et al., 2020)

## 419 2.4 Model Experiments

420

421 We conducted five experiments using the current Noah-MP driven by the hourly NLDAS-2 forcing  
 422 data at a spatial resolution of 0.125 degree, starting with the same uniform initial conditions—  
 423 namely, soil moisture at 0.3 m<sup>3</sup>m<sup>-3</sup> and soil temperature at 287K—spanning 2014 to 2019 for six  
 424 iterations. The initial five iterations were dedicated to the model's spin-up phase, and the resulting  
 425 surface and root zone soil moisture from the last iteration were used for SMM analysis. Parameters  
 426 were adopted per the updates by Niu et al. (2020), with adjustments to the dynamic vegetation  
 427 module to align with Moderate Resolution Imaging Spectroradiometer (MODIS) leaf area index  
 428 observations. This study refrained from parameter calibration related to dual-domain schemes for  
 429 preferential flow (Šimůnek & Van Genuchten, 2008) and ponding depth.

430

431 The five experiments are conducted with Noah-MP configurations with different water retention  
 432 and infiltration schemes. Table 1 lists optional schemes that were the same for all these  
 433 experiments. for other processes, including surface layer turbulent exchange, radiation transfer,  
 434 phase changes between snow and rain, and the permeability of frozen soil. For this study, we  
 435 selected only those schemes that have a direct impact on the simulation of soil moisture dynamics  
 436 (as detailed in Table 2). All these experiments are set with the same number of soil layers, which  
 437 vary spatially from 5 – 15 vertical layers with fixed layer thicknesses:  $\Delta z_i = 0.05, 0.3, 0.6, 1.0, 2.0,$

438 2.0, 4.0, 4.0, 5.0, 5.0, 5.0, 5.0, 5.0, 5.0, and 5.0 m down to 49.0 m to match the maximum bedrock  
 439 depth data of Pelletier et al. (2016) with a minimum bedrock depth of 4.0 m. The model was  
 440 customized using a combination of three soil moisture solver variants, two soil hydraulics schemes,  
 441 and two ponding depth thresholds.

442  
 443 To explore the influence of surface ponding on SMM, we designed two distinct experimental  
 444 conditions. The first condition, designated as MF\_VGM0, excluded the ponding effect by setting  
 445  $H_{top,max}$  to 0 mm. Conversely, the second condition, identified as MF\_VGM200, incorporated a  
 446 significant ponding depth of 200 mm. Both conditions utilized the mixed-form RE solver alongside  
 447 the Van-Genuchten (VGM) model (refer to Table 2). Furthermore, we conducted comparative  
 448 analyses to assess the role of soil hydraulic properties by conducting experiments with the Brooks-  
 449 Corey/Clapp-Hornberger (BC/CH) model (MF\_CH) and the VGM model (MF\_VGM), each with  
 450 a ponding depth threshold of  $H_{top,max} = 50$  mm.

451 An additional experiment employs the Dual-Permeability model (DPM) within the VGM  
 452 framework, maintaining the same ponding threshold of  $H_{top,max} = 50$  mm, referred to as  
 453 DPM\_VGM (see Table 2). The comparison of DPM\_VGM with the MF\_VGM setup aimed to  
 454 shed light on the effects of preferential flow channels on soil moisture forecasting, and runoff  
 455 forecasting in future studies, thereby enhancing our comprehension of the complexities inherent  
 456 in hydrological modeling.

457  
 458 To define the macropore volume fraction, we used the modeled Soil Organic Matter (SOM), which  
 459 is computed from Noah-MP with a microbial-enzyme model (Zhang et al., 2014) prior to the major  
 460 experiments conducted in this study through a long-term (120 years) spin-up simulation from 1980  
 461 – 2019 driven by the NLDAS data. The modeled SOM shows a pattern of less SOM in wet regions  
 462 but more in arid regions due to more active microbial activities (decomposition and respiration) in  
 463 wetter regions. The resulting macropore volume fraction ranges from 0.05 – 0.15 changing with  
 464 spatially-varying SOM. While we conducted sensitivity analyses on key parameters such as the  
 465 ponding depth threshold and macropore fraction to identify ranges yielding realistic outcomes, we  
 466 acknowledge that further model development (building relationships with global high-resolution  
 467 DEM and soil data, e.g., SoilGrids250m (Poggio et al., 2021) are necessary to refine the  
 468 parameters.

469  
 470 Table 2 Model experiment configuration.

Experiment ID	Models	$H_{top,max}$ (mm)	Soil Hydraulics
MF_VGM0	Mixed Form RE	0	Van-Genuchten
MF_VGM200	Mixed Form RE	200	Van-Genuchten
MF_CH	Mixed Form RE	50	Brooks-Corey/Clapp-Hornberger
MF_VGM	Mixed Form RE	50	Van-Genuchten
DPM_VGM	DPM	50	Van-Genuchten

471

### 472 3. Results

473

474 In Sections 2.1 and 2.2 of our study, we focus on computing the SMM for both the surface (5 cm)  
475 and root zone (up to 1m) layers, respectively. This dual-layer analysis is fundamental to our  
476 experiments as it allows us to understand the differential impacts of various parameterizations on  
477 soil moisture. By comparing and analyzing the SMM values across these two distinct layers, we  
478 can identify specific physical processes that influence soil moisture dynamics. This comparative  
479 approach not only elucidates how these processes affect SMM but also helps in understanding the  
480 interaction between surface characteristics and subsurface moisture dynamics, which are critical  
481 for improving hydrological modeling and prediction.

482

#### 483 3.1 Long- and Short-Term Soil Moisture Memory of the Surface Layer

484

485 Figure 3 illustrates the spatial distribution of median long-term memory, derived from the five-  
486 year soil moisture dataset. We also provide plots for the SMM spatial distributions to offer insights  
487 for each model experiments. However, it turns out that interpreting the fundamental mechanisms  
488 behind the distribution is very challenging regarding the spatial distributions of other controlling  
489 factors, e.g., climatic forcing, vegetation/soil type, elevation, slope angle/aspect (affecting solar  
490 radiation), which directly or indirectly controls actual ET and runoff as well as interactions  
491 between ET and soil moisture (Rahmati et al., 2024). As such, we focus on comparing the median  
492 SMM values across model scenarios to find the dominate hydrological processes controlling  
493 SMM, because the modeled distributions from the different experiments generally show the same  
494 shape, especially for the same hydraulics (e.g., VGM). Analysis of the SMAP data revealed that  
495 long-term memory ( $\tau_L$ ) is significantly higher in the energy-limited and humid regions of the  
496 eastern US, and lower in the arid western regions. These findings are consistent with those of He  
497 et al. (2023) and McColl et al. (2019).

498

499 The MF\_CH experiment displays a spatial pattern that contrasts with the SMAP data, with a longer  
500 memory in the arid western regions but a shorter memory in the wet northeastern regions (Figure  
501 3a & 3b). This is likely caused by the faster drainage of topsoil water under the wetter conditions,  
502 whereas under the drier conditions, the spuriously stronger suction from the CH hydraulics sustain  
503 the surface soil moisture for a longer period. Further examination reveals that models using the  
504 Van-Genuchten scheme reflect SMAP's patterns. Specifically, the eastern regions display higher  
505  $\tau_L$  values, while the western regions show lower values (see Figure 3b-f). DMP\_VGM  
506 demonstrates a shorter memory in the eastern CONUS compared to MF\_VGM (refer to Figures  
507 3c, d, and S1. VGM scenario with zero ponding depth shows a shorter memory compared with  
508 MF\_VGM200 in the eastern CONUS (Figures 3e and f), where surface ponding happens more  
509 frequently and with a greater depth. Figure S2 shows a better match of data points with the  
510 agreement line in the DPM\_VGM versus SMAP scatterplot. In contrast, the MF\_CH versus SMAP  
511 scatterplot lacks this alignment with a correlation of  $-0.10$ . The correlation values have risen from  
512  $-0.10$  to  $0.15$  with VGM, a sign of progress, but they are still not strong.

513

514

515

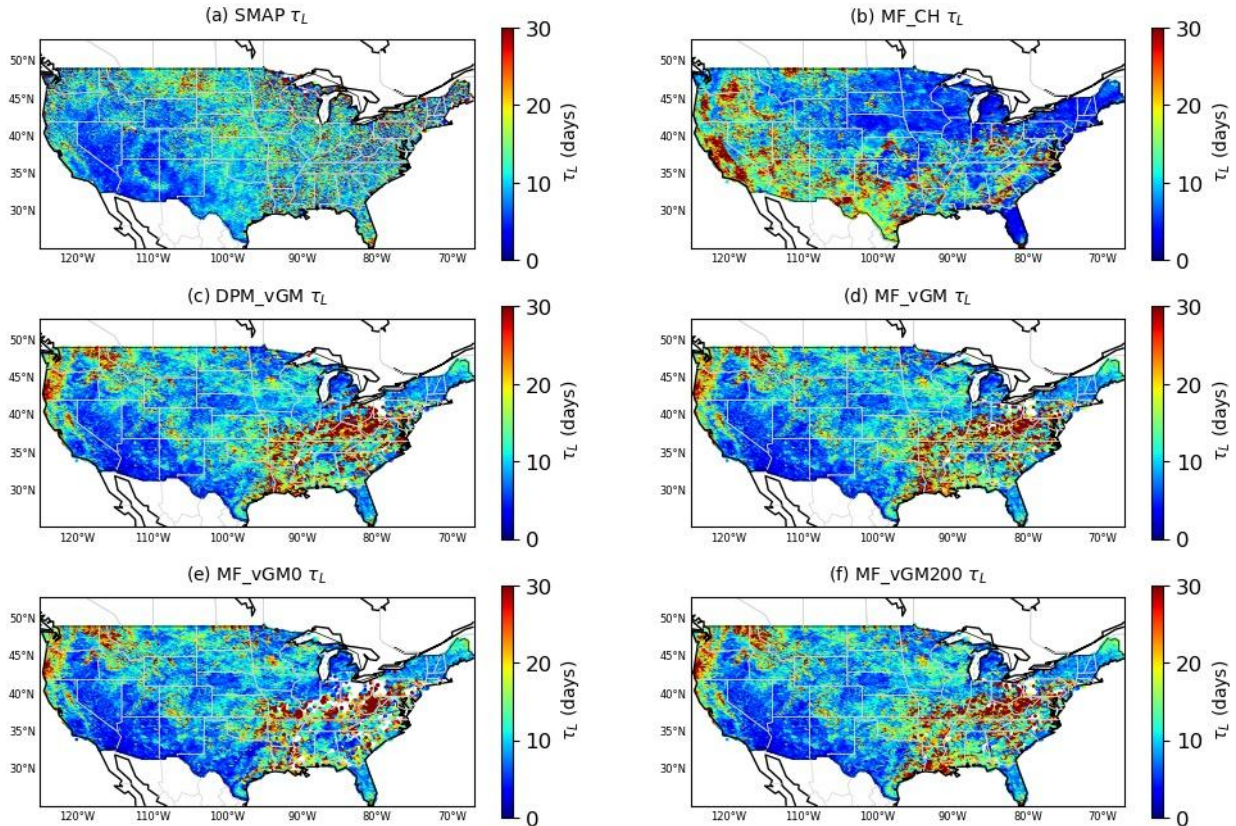


Figure 3. Long-term SMM derived from various datasets from 2015 – 2019 for soil surface layer: (a) SMAP; (b) MF\_CH; (c) DPM\_VGM; (d) MF\_VGM; (e) MF\_VGM0; and (f) MF\_VGM200. SMM = Soil Moisture Memory

516

517 To assess the influence of plant water storage on SMAP soil moisture data and the resultant SMM,  
 518 we employed the MODIS NDVI to categorize the entire CONUS into wet ( $NDVI > 0.45$ ) and dry  
 519 regions ( $NDVI < 0.45$ ). In the dry areas (see Figure 4a), the probability distribution function (PDF)  
 520 of the surface SMM from MF\_CH differs from that of SMAP and exhibits a higher median of  
 521 10.53 days compared to SMAP's 8.47 days (overestimation). Other model scenarios using van  
 522 Genuchten (VG) hydraulics, with an SMM median of around 8.6 days, show a distribution PDF  
 523 like SMAP. Note that the VGM scenarios effectively tackle the problem of long-term memory  
 524 overestimation, a point emphasized by He et al. (2023). This improvement is due to the refined  
 525 parametrization of physical processes within the VGM experiments.

526

527 In the wet regions with dense vegetation (Figure 4b), the SMM PDF of MF\_CH (median of 8.03  
 528 days) significantly varies from the SMAP PDF (median of 10.71 days), showing an  
 529 underestimation of  $\tau_L$ . However, due to the strong effect of plant water storage on the SMAP's soil  
 530 moisture retrieval (commonly in the eastern CONUS), our focus here is on model sensitivity to  
 531 process representations rather than on model accuracy relative to SMAP data. Other models with  
 532 the van Genuchten (VG) scheme display greater variability among themselves in wet areas (Figure  
 533 4b) than in the dry region (Figure 4a). MF\_VGM0 (with a zero ponding depth threshold) shows a  
 534 shorter long-term SMM, with a median of 10.72 days, compared to MF\_VGM200 (with a 200 mm

535 threshold), with median of 12.05 days, and MF\_VGM (with 50 mm ponding threshold), with a  
 536 median of 12.03. This suggests extra water inputs from the surface ponded water (MF\_VGM200)  
 537 can help extend the surface SMM. Changing the ponding depth threshold from 50 mm (MF\_VGM)  
 538 to 200 mm (MF\_vGM200), has a marginal effect on  $\tau_L$ , suggesting that the response does not  
 539 proportionally increase with higher values. With the same 50 mm ponding threshold, DPM\_VGM  
 540 produces a shorter SMM, with a median of 11.73 days, than MF\_VGM, indicating that the effects  
 541 of faster water drainage of the topsoil water caused by the preferential flow (as represented by  
 542 DPM\_VGM) can last longer.  
 543

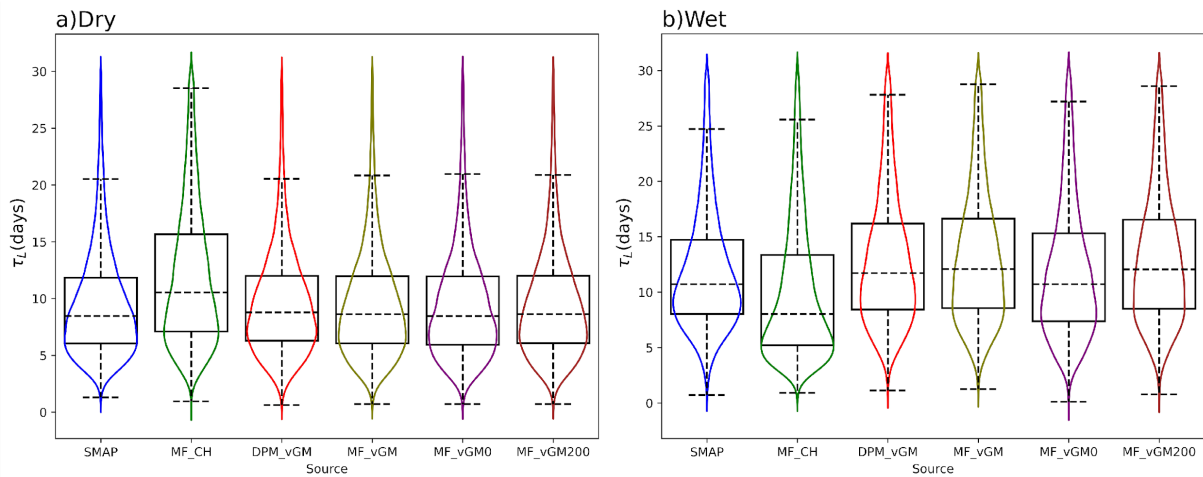


Figure 4 Violin plot of surface  $\tau_L$  estimated from SMAP and Noah-MP scenarios for dry regions with less vegetation ( $NDVI < 0.45$ ) and wet regions with more vegetation ( $NDVI > 0.45$ ).

544  
 545 For the short-term SMM, all the scenarios produce an overall spatial pattern similar to that of the  
 546 SMAP-derived  $\tau_s$ , showing a longer memory in the drier western US than in the wetter eastern  
 547 (Figure 5). However, MF\_CH shows a shorter memory in the northwestern US than that derived  
 548 from SMAP (Figure 5a & b). MF\_CH with a median of 1.9 days underestimates SMAP with a  
 549 median of 2.02 days, while VG scenarios have median  $\tau_s$  around 2.09 days over dry regions. This  
 550 effectively rectifies the underestimation in short-term memory by LSMs, as reported in previous  
 551 studies (He et al., 2023). He et al. (2023) highlighted that most LSMs tend to underestimate  $\tau_s$ ,  
 552 which is strongly affected by soil water drainage as specified by McColl et al. (2019). Note that  
 553 higher  $\tau_s$  values indicate slow drainage, whereas lower values suggest faster drainage; this is  
 554 exemplified by Figure 5a, which exposes a more rapid drainage in the eastern CONUS in contrast  
 555 to the western. The incorporation of surface ponding and DPM (2.08 days) has shown less effects  
 556 on short-term memory than the soil hydraulics for the dry region (more macropores are available  
 557 in wet regions and hence DPM would have more effect in those regions). The introduction of  
 558 surface ponding (comparing MF\_VGM0 (2.11 days) to MF\_VGM200 (2.108 days) in Figure 5  
 559 and Figure 6) contributes to more persistent surface soil moisture and a bit faster drainage. The  
 560 pdf of SMM from all the VGM models more closely resembles the SMAP pdf in the western  
 561 United States than in the eastern part of the country due likely to that the SMAP soil moisture  
 562 retrieval may be affected by the plant water storage and thus the spatial variations in canopy  
 563 density.  
 564



565 For wet regions, MF\_CH with a median of 1.26 days underestimate SMAP with a median of 1.56  
566 days. DPM\_VGM with faster drainage of surface soil water produces a median  $\tau_s$  of 1.43, shorter  
567 than does MF\_VGM with a median of 1.48 days. The DPM model accelerates the drainage of  
568 water from the topsoil. This effect is more significant in the eastern CONUS. As a result, it lowers  
569 the short-term memory in areas where the soil has macropores.

570

571 The modeling results also indicate the long-term memory of the surface soil moisture is more  
572 sensitive to the four VGM schemes in the wet regions (Figure 4b) than the short-term memory (  
573 Figure 6b). This can be attributed to the differences in how topsoil water responds to surface  
574 ponding and preferential flow as represented by the four VGM across different moisture regimes.  
575 Under higher soil moisture conditions right after a rainfall event, the persistence of soil moisture  
576 is mainly dominated by drainage of topsoil water to deeper soil, whereas at relatively lower soil  
577 moisture, the long-term memory is more controlled by persistent water inputs from surface ponded  
578 water and prolonged drainage by preferential flow. This also indicates that the effects infiltration  
579 of surface ponded water and preferential flow can last longer up to more than 10 days. Under dry  
580 conditions (Figure 4a and 6a), these hydrological processes become less important. However, the  
581 soil water retention curves as represented by the CH and VG schemes play a more important role  
582 under any conditions (Figure 4a and Figure 6a). Another possible reason can be the issue of time  
583 scale. Short-term memory has values up to 5 days, and given the SMAP revisit time of 3 days,  
584 generating values for intervals shorter than 3 days may challenge the validity of short-term  
585 memory as a reliable measurement for soil drainage, as demonstrated by McColl et al. (2019).  
586 Since we selected Noah-MP days corresponding to the SMAP revisit time, it is possible that the  
587 effects of different VG parameterizations were diminished by this sampling. We suggest that other  
588 measurements, such as streamflow and baseflow analysis, should be considered to better quantify  
589 the effect of soil hydraulics on soil drainage. Ji et al. (2023) demonstrated that high-resolution soil  
590 datasets and model parameterizations can enhance these synergistic effects (Ji et al., 2023). This  
591 variation in how local environmental conditions are represented likely explains the greater  
592 variability observed in wet regions in Figure 4.

593

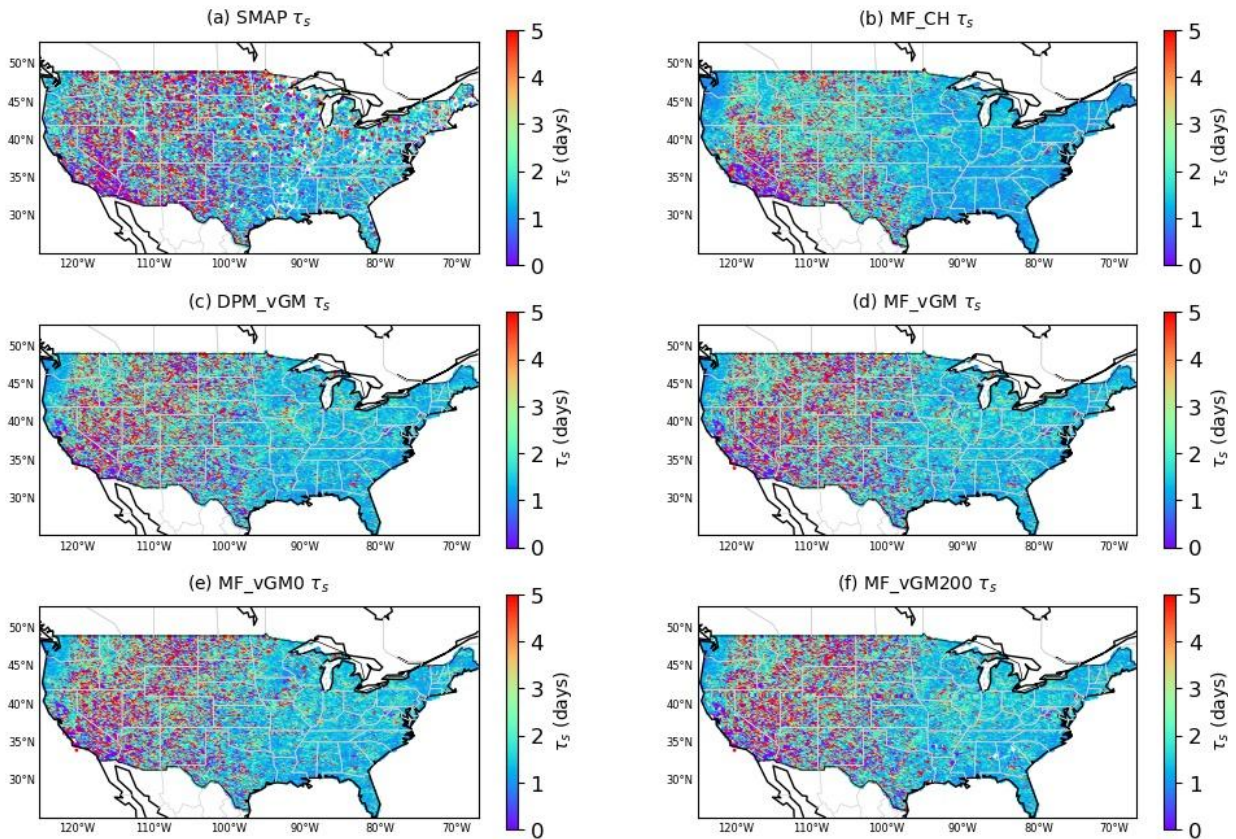


Figure 5 Short-term SMM derived from various datasets from 2015 – 2019 for soil surface layer: (a) SMAP; (b) MF\_CH; (c) DPM\_vGM; (d) MF\_vGM; (e) MF\_vGM0; and (f) MF\_vGM200. SMM = Soil Moisture Memory.

594

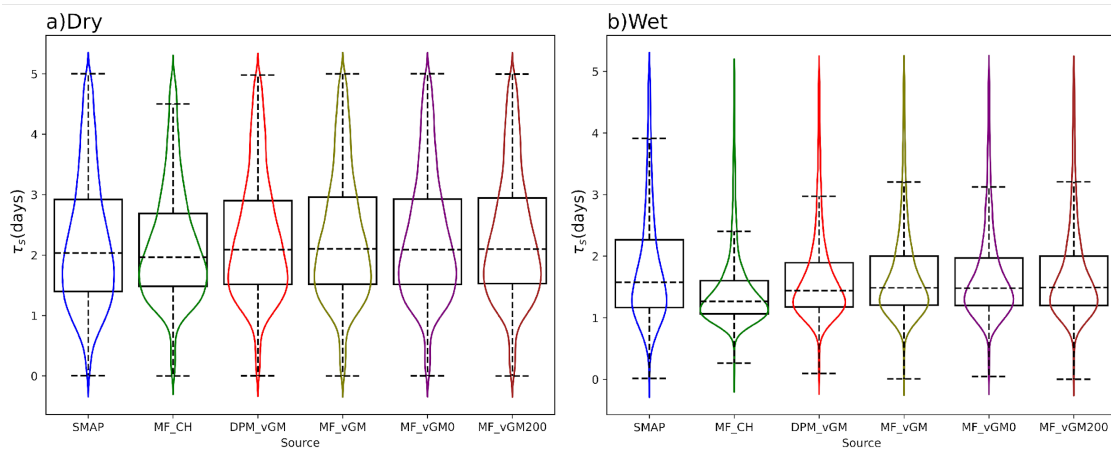


Figure 6 Same as Figure 4 for short-term memory.

595

### 596 3.2 Long- and Short-Term Soil Moisture Memory of the Root Zone Layers

597

598 We use the International Soil Moisture Network (ISMN) soil moisture dataset as the benchmark  
 599 and compute SMM at the ISMN stations as illustrated in Figure 2. We compute the long-term  
 600 SMM across 654 sites within CONUS for the period from 2015 – 2019. The median values of  
 601 these computations indicate that the root zone SMM (Figure 7 & Figure 9) is generally higher than  
 602 the surface SMM (Figure 3 & Figure 5). Analysis of ISMN data reveals that the root zone  $\tau_L$  (Figure  
 603 7) generally exceeds surface  $\tau_L$  (Figure 3), particularly longer in the western US. Some eastern  
 604 locations also exhibit longer  $\tau_L$ , whereas the central region demonstrates lower values.

605  
 606 MF\_CH produces a shorter root-zone  $\tau_L$  across nearly all the sites in CONUS (Figure 7 & Figure  
 607 8). The Van-Genuchten scheme mirrors the ISMN-derived  $\tau_L$ , albeit with slightly higher values  
 608 (Figure 7 & Figure 8). An increase in surface ponding depth raises the  $\tau_L$ . This is particularly true  
 609 in the eastern US, where surface ponding occurs more often, and its impact on soil moisture is  
 610 more substantial. Figures S3 and S4 illustrate this effect. Additionally, DPM\_VGM (Figure 7c and  
 611 Figure 8) reduces the root-zone long-term SMM across most of CONUS relative to the other  
 612 models (Figure 7c, d, e, & f and Figure S3).

613

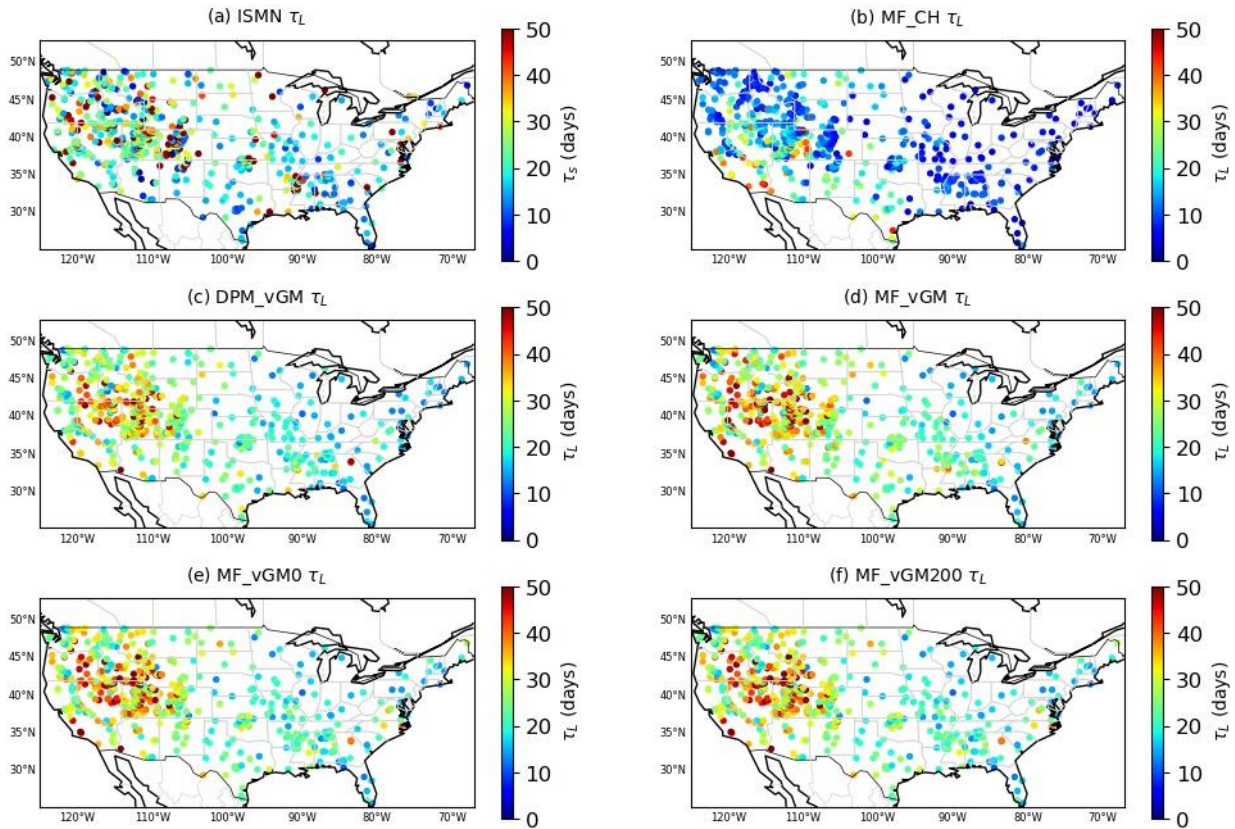


Figure 7 Long-term root-zone SMM derived from various datasets from 2015 – 2019: (a) ISMN; (b) MF\_CH; (c) DPM\_VGM; (d) MF\_VGM; (e) MF\_VGM0; and (f) MF\_VGM200. SMM = Soil Moisture Memory.

614  
 615

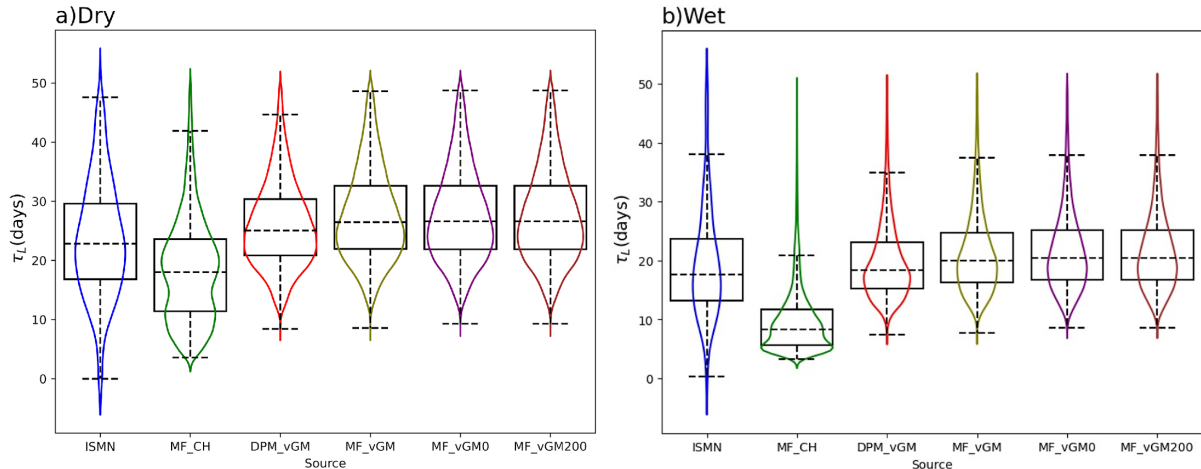


Figure 8 Violin plot of root zone  $\tau_L$  estimated from ISMN and Noah-MP scenarios for dry regions with less vegetation (NDVI < 0.45) and wet regions with more vegetation (NDVI > 0.45).

616 As for the surface layer, we use the MODIS NDVI to classify all the stations into wet and dry  
 617 regions. In the dry regions (Figure 8a), MF\_CH has a different probability distribution function  
 618 and a lower median of 19 days compared to that of ISMN (median of 23 days). All the other  
 619 scenarios using VG schemes exhibit a similar SMM PDF to each other, yet they are somewhat  
 620 different from the one derived from ISMN. Also, the presence of macropores reduces long-term  
 621 SMM, with a median of 25 days, and results in the closest median to the ISMN (Figure 8a). ISMN,  
 622 however, shows a large range of long-term SMM compared with all the Noah-MP experiments,  
 623 indicating the complex nature of the observed SMM needs further investigation (Figure 8a & b).  
 624 Note that the analyses were conducted at a limited number of locations, presenting challenges in  
 625 fully capturing the impacts of different parameterizations on SMM.

626

627 In the wet regions, MF\_CH shows smaller  $\tau_L$  values (median of 9.8 days) than that from ISMN  
 628 (median of 18 days) together with a noticeable pdf difference. The effect of dual permeability  
 629 decreases the soil moisture and long-term memory compared with the other model experiments,  
 630 resulting in a median (19 days) close to ISMN (18 days), Figure 8b. However, it seems that the  
 631 ponding depth does not show a noticeable impact on  $\tau_L$ . It should be noted that the effect of ponding  
 632 depth, which slightly increases the long-term memory in RTZ, can be observed in Figure S3 and  
 633 Figure S4 when we take a close look into them.

634

635 Further investigation reveals an enhancement in the model's ability to capture soil hydraulic  
 636 dynamics when shifting from the Clapp-Hornberger to the Van-Genuchten scheme, with an  
 637 improvement in  $\tau_L$  values from 0.05 to 0.12 (Figure S5). Also, The Dual Permeability model with  
 638 Van-Genuchten (DPM\_VGM) demonstrates superior performance with a correlation of 0.15,  
 639 compared to all other scenarios tested.

640

641

642

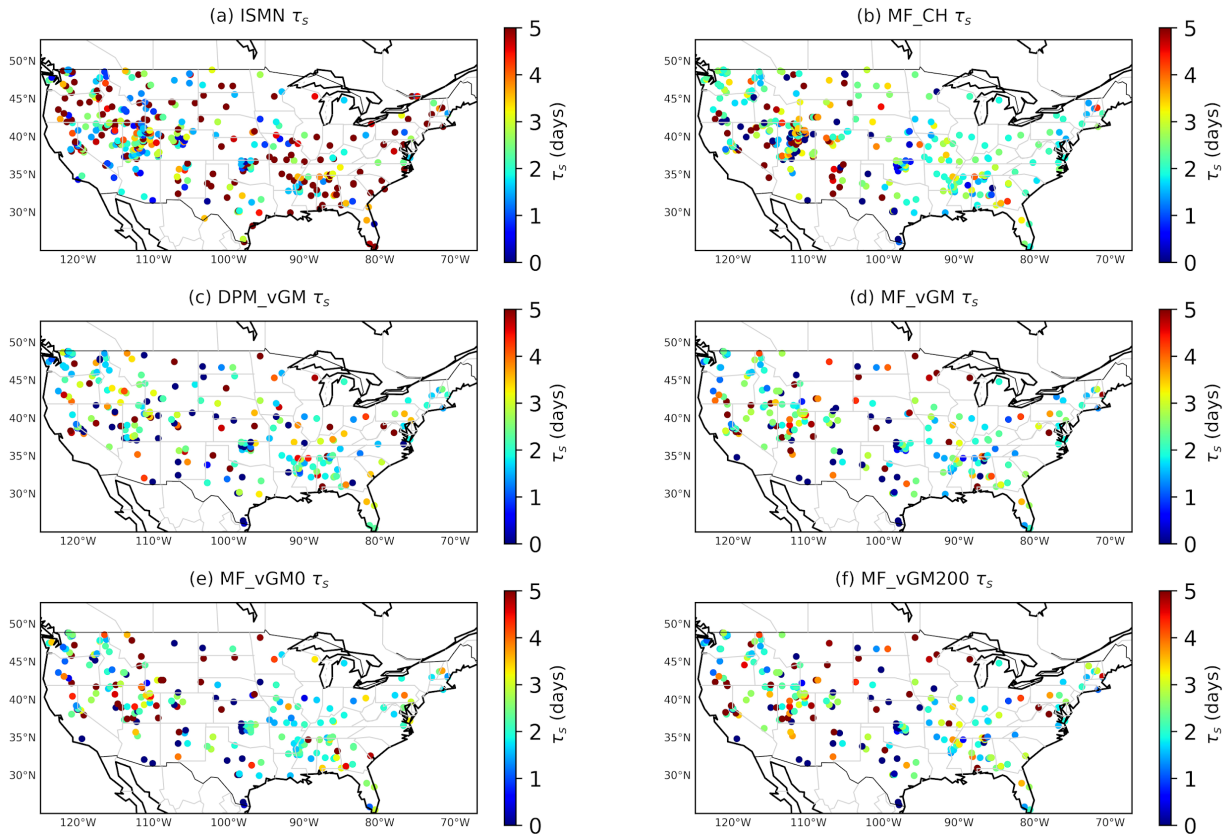


Figure 9 Same as Figure 7 but for short-term.

643

644 The findings show that  $\tau_s$  in most Noah-MP scenarios are comparable to those observed in the  
 645 ISMN data, as shown in Figure 9b to f. However, there is a consistent underestimation in some  
 646 eastern locations. Figure 10 highlights this pattern, showing that wet regions tend to underestimate  
 647  $\tau_s$ , with ISMN reporting a median of 2.5 days and Noah-MP experiments a median of around 2  
 648 days. Conversely, dry regions tend to overestimate, with ISMN at a median of 2.1 days and Noah-  
 649 MP experiments at approximately 2.7 days.

650

651 Although distinguishing between MF\_vGM0 and MF\_vGM200 in Figure 9 and Figure 10 is  
 652 challenging, Figure 11 (Figure 11c and d) reveals that an increase in ponding depth leads to a slight  
 653 decrease in short-term memory in the eastern CONUS. Comparing Figure 9 with Figure 11  
 654 indicates that ISMN stations partially reflect the spatial pattern of long-term and short-term  
 655 memory in the root zone across CONUS. It may be concluded that the spatial patterns of long-  
 656 term and short-term memory (Figure 11 and Figure S7) of the root zone are quite similar to those  
 657 of the surface layer (Figure 3 and Figure 5). Hence, long-term memory is more prevalent in the  
 658 eastern CONUS and mountainous areas, while longer short-term memory occurs predominantly  
 659 in western areas. However, this conclusion is not totally true and further investigation is needed.

660

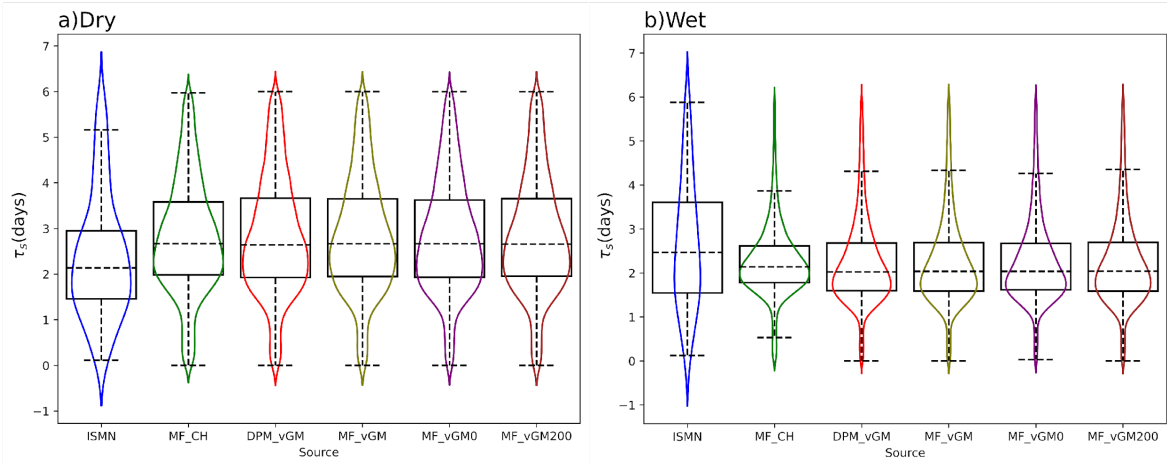


Figure 10 Same as Figure 8 but for the short-term SSM.

661  
662

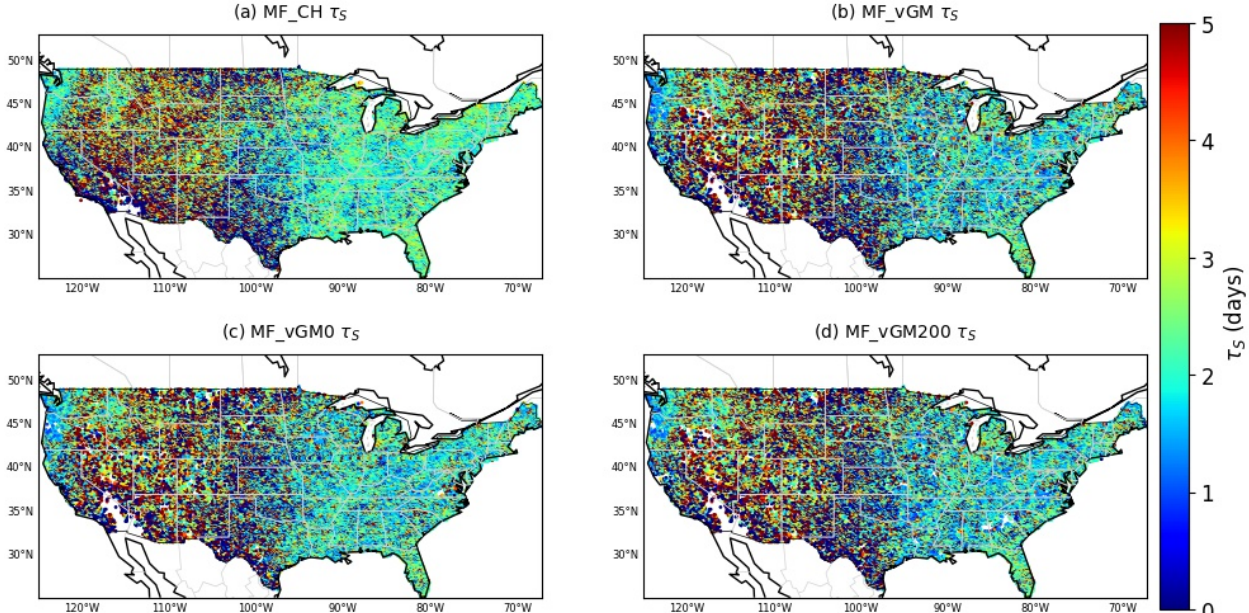


Figure 11 Spatial distribution of root zone  $\tau_s$  estimated from (a) MF\_CH; (b) MF\_vGM; (c) MF\_vGM0; and (d) MF\_vGM200.

663 **4. Discussion**

664 **4.1 How Do Different Parametrizations Affect SMM?**

665  
666 The efficacy of LSMs in simulating climate feedback mechanisms critically depends on the soil's  
667 ability to retain moisture and how fast the soil releases the moisture up to the atmosphere through  
668 soil surface evaporation and plant transpiration and down to the aquifers through recharge. The  
669 rapid infiltration of incident water (rainfall and snowmelt) into deeper subsoil strata reduces the  
670 soil's capacity to return moisture to the atmosphere through evaporation and transpiration. Thereby

671 disrupting potential atmospheric feedback loops in LSMs (Mccoll et al., 2019). Conversely, If  
672 LSMs lose water too quickly through ET, they provide feedback to the atmosphere faster than they  
673 should. Thus, the concept of SMM becomes essential in LSMs, as it can provide information about  
674 the rate at which moisture disappears from soil. Hence, understanding the effects of various  
675 physical processes on SMM is vital for enhancing the representation of these processes in LSMs,  
676 thereby improving their overall performance in simulating the complex interactions between the  
677 land surface and the atmosphere.

678

679 The water retention curve characteristics of the BC/CH hydraulics scheme are characterized by a  
680 strong suction force that is more pronounced than in the Van-Genuchten model for various soil  
681 types (Niu et al, 2024). This stronger suction promotes moisture transfer from the deeper layers to  
682 the surface layer, causing the surface soil to retain more moisture (Figure S6) and has a longer  $\tau_L$   
683 (Figure 3, 4), a common issue in LSMs according to He et al. (2023). Moreover, the higher suction  
684 reduces the root zone moisture and consequently, it would have a shorter  $\tau_L$  (Figure 7 and 8).  
685 Conversely, the VG scheme, with weaker suction, transfers less moisture from the root zone to the  
686 surface, resulting in a drier surface layer and a shorter  $\tau_L$  for the surface, but a longer  $\tau_L$  for the root  
687 zone, as depicted in Figures 7 and 8.

688

689 Short-term memory is inversely related to moisture availability; thus, a wetter soil has a shorter  $\tau_S$ ,  
690 whereas a drier layer has a longer  $\tau_S$ . The VG scheme produces a drier surface layer and a moister  
691 root zone, leading to a longer surface  $\tau_S$  but a shorter root zone  $\tau_S$  compared to the BC/CH scheme,  
692 as shown in Figures 5, 6, and 11.

693

694 As indicated in a previous study (He et al., 2023), a common issue in LSMs is the overestimation  
695 of the long-term memory of surface soil over dry regions. This could be attributed to  
696 underestimation of evaporation within LSMs using the CH parametrization (Figure S7a), resulting  
697 in overestimation of soil moisture. However, a shift towards the VG scheme increases the  
698 evaporation (Figure S7b, Figure S8), and hence it overcomes the  $\tau_L$  overestimation (Figure 3 and  
699 4).

700

701 The presence of soil macropores promotes infiltration at the soil surface and rapid flow through  
702 preferential pathways from the surface to the root zone (Mohammed et al., 2021), consequently  
703 reducing the moisture retained in the surface layer. Moreover, macropores lead to reduced suction  
704 of the soil, hence less water from subsurface soil was pulled up to the surface, causing the topsoil  
705 to have less moisture (Figure S6). Therefore, macropores lead to a decrease of surface  $\tau_L$ (Figure  
706 3d, 4b). Moreover, the presence of macropores increases the root-zone soil moisture and  
707 consequently, it should prolong the root zone  $\tau_L$ . However, the even distribution of macropores  
708 throughout the soil profile in current Noah-MP configuration, DPM\_VGM, increases water  
709 infiltration into deeper layers, resulting in faster flow to deep soil layers, recharge to groundwater  
710 and thus a drier root zone. As a result, macropores reduce the root-zone long-term SMM (Figure  
711 7d, e, & f and Figure S8) of DPM\_VGM. This highlights the importance of calibration of  
712 macropore profile in DPM\_VGM for better representations of macropore effects and soil  
713 hydrohalic dynamics.

714

715 While the soil matrix typically allows for only slow water movement due to the pressure gradient,  
716 macropores enable rapid gravitational flow (Mohammed et al., 2018). These macropores facilitate

717 quicker infiltration to the root zone (Mohammed et al., 2021). Therefore, they increase the drainage  
718 rate to these deeper layers, which slightly reduces the short-term soil moisture memory in the  
719 surface (Figures 5 and 6). Additionally, as water moves from the surface to the root zone, the  
720 increased moisture content there leads to quicker drainage (we speculate that this occurs in the real  
721 world; however, in the current DPM\_VGM, the deep soil is wetter than root zone, indicating a  
722 need for calibration of the macropore profile as we have stated). Consequently, this process further  
723 decreases the short-term moisture memory in the root zone due to the higher drainage rates of  
724 wetter soil.

725

726 Finally, the ponding threshold allows water to remain on the surface before turning into runoff.  
727 This provides water with more time to percolate into the soil. The consequent increase in ponding  
728 depth allows extended water infiltration, thus enhancing soil moisture and lengthening moisture  
729 retention through the soil profile (Figure S6e, f). So as discussed before, wetter soil leads to  
730 prolonged  $\tau_L$  and shorten  $\tau_S$  (Figure 5, 6, 7, 11).

731

## 732 **4.2 Limitation of Our Study**

733

734 Some sources of uncertainty may affect our results in this study, including uncertainties in input  
735 data, and models. The SMAP L-band penetration depth can indeed be shallower than 5 cm,  
736 especially over wetter regions like the eastern CONUS, which may introduce a mismatch when  
737 comparing SMAP observations with the Noah-MP 5 cm layer. SMAP reliability is affected by  
738 plant water storage change (in the eastern part and some mountainous sites), introducing  
739 uncertainties into SMM values for the benchmark. While SMAP observations may be less reliable  
740 over these densely vegetated areas, they still support our objective of enhancing our understanding  
741 of the physical processes in soil hydrology. Furthermore, the SMM patterns captured from SMAP  
742 can be insightful in understanding regional variabilities in SMM.

743

744 Another concern is the influence of ISMN spatial representation on SMM analysis. ISMN stations  
745 are point-based, and it is assumed that one point represents a 1/8-degree grid area. It is possible  
746 that the point measurements cannot fully capture the spatial variability within the Noah-MP grid  
747 cells, leading to discrepancies in the representation of values and spatial patterns. The limited  
748 number of stations may further amplify this issue. One potential solution to address the scale  
749 mismatch between point-based observations and grid-scale simulations is the use of high-  
750 resolution or hyper-resolution models. These models can provide finer spatial detail, allowing for  
751 a more direct comparison between observational data and model outputs, thereby improving the  
752 accuracy of the analysis and reducing scale-induced biases. Incorporating such approaches in  
753 future studies would help mitigate the limitations posed by the current scale differences.

754

755 Additionally, some model representations may require further investigation. The DPM\_VGM  
756 scheme uses vertically constant macropore volume fraction, which means macropores generated  
757 by biotic factors (formed by wormhole and dead roots) and abiotic factors (cycles of freezing-  
758 thawing and drying-wetting) are fixed down to the bedrock. However, in nature, these macropores  
759 would reduce after a few meters from the soil surface. Because the existence of macropores in  
760 nature drains the surface layer and increases the root zone soil moisture, to better represent the  
761 actual physical process, it is necessary to incorporate more soil data, e.g., the soil organic matter  
762 and coarse materials from e.g., SoilGrid250m for climate predictions or calibrate macropore



763 volume fraction for hydrological applications. Such a calibration is anticipated to further advance  
764 the fidelity of soil moisture simulations, enhancing the model's utility in various hydrological and  
765 climate applications.

766  
767 Concerning surface water ponding, a constant ponding threshold may not be justified, and a  
768 spatially variable surface ponding may lead to improved model accuracy. Future model  
769 developments should consider micro-scale topographic variations to represent the hydrologic  
770 connectivity of surface ponded water. We tested a scheme of ponding threshold as a linear function  
771 of the subgrid standard deviation of DEM derived from DEM at 30 m resolution (not enough  
772 though), resulting larger surface ponding thresholds over the alpine west US. Further investigation  
773 is needed to validate and calibrate the modeled areal ponding fraction and depth against satellite  
774 (or camera) derived. We expect a more realistic representation of ponding threshold through  
775 further calibration of the parameters in the function.

776  
777 There are additional factors, such as water convergence through surface and subsurface lateral  
778 flows, that may affect SMM but are not represented by the current Noah-MP version and thus not  
779 considered in our analysis. The primary focus of our study is to understand the impacts of missing  
780 processes on SMM and use this understanding to guide future LSM development for S2S climate  
781 predictions, for instance, the surface ponding and preferential flow. Consequently, we narrowed  
782 our examination down to key missing processes represented within Noah-MP. Future research  
783 would further evaluate the impact of lateral flows and other processes on SMM, expanding our  
784 understanding of these dynamics and their implications for climate prediction. Moreover, this  
785 study focuses primarily on physical process representations and parameterizations for soil moisture  
786 dynamics, while we acknowledge the strong impacts of uncertainties in hydraulic parameters.

## 787 **5. Conclusion**

788  
789 In this study, we have explored the effects of soil hydraulic schemes and hydrological processes  
790 on SMM using the Noah-MP LSM with advanced hydrology. Our research was motivated to  
791 understand how missing physical processes help solve the commonly observed biases in long-  
792 term/short-term SMM by LSMs. We aim to find the key missing processes controlling SMM and  
793 thus to improve the representation of soil hydrology in LSMs, using the knowledge gained from  
794 our analysis of SMM. We designed and implemented five scenarios to focus on the impacts of key  
795 missing processes and different hydraulic parameterizations. These scenarios include two soil  
796 hydraulic models (Clapp and Hornberger and Van-Genuchten), a dual permeability model  
797 representing preferential flow, and three surface ponding thresholds. Using soil moisture datasets  
798 from SMAP and ISMN for surface and root zone measurements, respectively, we conducted a  
799 comprehensive analysis of the effects of different Noah-MP parameterizations on soil moisture  
800 memory.

801  
802 Our findings suggest that the soil water retention curve is the most important factor controlling  
803 SMM, due to its strong influence on soil water persistence through suction by the soil particles.  
804 We show that the adoption of the Van-Genuchten (VG) parameterization considerably mitigates  
805 the long-standing issue of overestimating SMM in LSMs employing the Brooks-Corey/Clapp-  
806 Hornberger (BC/CH) hydraulic model. The Van-Genuchten model, with its reduced suction effect  
807 attributable to a drier surface layer, leads to a more accurate depiction of moisture transfer from

808 the root zone to the surface, which is important for more realistic description of soil moisture  
809 dynamics.

810  
811 Moreover, representing surface ponding processes allows for an extended period of soil water  
812 infiltration, thus extending both surface and root-zone long-term memories and reducing the short-  
813 term memory. Implementing a dual-permeability approach fine-tunes soil moisture representation  
814 by accounting for preferential flow paths, marking a step forward in the enhancement of soil  
815 moisture memory and the overall fidelity of hydrological simulations. Macropores lead to a  
816 decrease in short-term memory and long-term memory, due to faster drainage and thus decreased  
817 surface soil moisture. Given these compelling advancements, we strongly recommend that LSMs  
818 adopt the VG hydraulics to advance the prediction of hydrological and climatic phenomena.

819  
820 The findings from this study have important implications for future research on SMM. By  
821 identifying the specific parameterizations that lead to discrepancies in long-term and short-term  
822 SMM, future studies should focus on refining these parameters to reduce biases in LSMs.  
823 Moreover, while this study focuses on the effect of the missing hydrological processes on the  
824 timescale of SMM, future research should analyze the impact of these parameterizations on the  
825 strength and legacy of SMM and assess whether the findings based on timescale align with those  
826 related to strength and legacy (Rahmati et al., 2024).

827  
828  
829  
830

### 831 **Competing interests**

832  
833 The contact author has declared that none of the authors has any competing interests.

### 834 **Acknowledgments**

835  
836 Funding for this project was provided by the National Oceanic and Atmospheric Administration (NOAA), awarded to  
837 the Cooperative Institute for Research on Hydrology (CIROH) through the NOAA Cooperative Agreement with The  
838 University of Alabama, NA22NWS4320003. Also, the research carried out for this article was supported by the U.S.  
839 Army Corps of Engineers, Engineer Research and Development Center, Coastal Inlets Research Program via  
840 Congressionally Directed R&D with the National Oceanic and Atmospheric Administration's National Water Center.  
841 The data used in this study are freely available online:  
842 NLDAS-2 data (<http://www.emc.ncep.noaa.gov/mmb/nldas/>); NASA SMAP soil moisture product  
843 ([https://nsidc.org/data/spl3smp\\_e/versions/6](https://nsidc.org/data/spl3smp_e/versions/6)); GPM IMERG-Final product  
844 ([https://disc.gsfc.nasa.gov/datasets/GPM\\_3IMERGHH\\_06/summary](https://disc.gsfc.nasa.gov/datasets/GPM_3IMERGHH_06/summary)). The Noah-MP code used in this study has  
845 been uploaded to a repository that may be accessed by other researchers  
846 ([https://github.com/mfarmani95/NoahMP\\_Dual](https://github.com/mfarmani95/NoahMP_Dual)).

847  
848  
849

### 850 **Reference**

851 Agnihotri, J., Behrangi, A., Tavakoly, A., Geheran, M., Farmani, M. A., & Niu, G. Y. (2023). Higher Frozen Soil  
852 Permeability Represented in a Hydrological Model Improves Spring Streamflow Prediction From River  
853 Basin to Continental Scales. *Water Resources Research*, 59(4). <https://doi.org/10.1029/2022wr033075>

- 854 Bisht, G., Riley, W. J., Hammond, G. E., & Lorenzetti, D. M. (2018). Development and evaluation of a variably  
855 saturated flow model in the global E3SM Land Model (ELM) version 1.0. *Geosci. Model Dev.*, *11*(10),  
856 4085-4102. <https://doi.org/10.5194/gmd-11-4085-2018>
- 857 Boone, A. (2004). The Rhône-Aggregation Land Surface Scheme intercomparison project: An overview. *17*, 187-  
858 208. [https://doi.org/https://doi.org/10.1175/1520-0442\(2004\)017<0187:TRLSSI>2.0.CO;2](https://doi.org/https://doi.org/10.1175/1520-0442(2004)017<0187:TRLSSI>2.0.CO;2)
- 859 Celia, M. A., Bouloutas, E. T., & Zarba, R. L. (1990). A general mass-conservative numerical solution for the  
860 unsaturated flow equation. *Water Resources Research*, *26*(7), 1483-1496.  
861 <https://doi.org/10.1029/WR026i007p01483>
- 862 Chen, F., & Dudhia, J. (2001). Coupling an Advanced Land Surface-Hydrology Model with the Penn State-NCAR  
863 MM5 Modeling System. Part I: Model Implementation and Sensitivity. *Monthly Weather Review*, *129*(4),  
864 569-585. [https://doi.org/https://doi.org/10.1175/1520-0493\(2001\)129<0569:CAALSH>2.0.CO;2](https://doi.org/https://doi.org/10.1175/1520-0493(2001)129<0569:CAALSH>2.0.CO;2)
- 865 Colliander, A., Jackson, T. J., Bindlish, R., Chan, S., Das, N., Kim, S. B., Cosh, M. H., Dunbar, R. S., Dang, L.,  
866 Pashaian, L., Asanuma, J., Aida, K., Berg, A., Rowlandson, T., Bosch, D., Caldwell, T., Caylor, K.,  
867 Goodrich, D., al Jassar, H., & Yueh, S. (2017). Validation of SMAP surface soil moisture products with  
868 core validation sites. *Remote Sensing of Environment*, *191*, 215-231.  
869 <https://doi.org/https://doi.org/10.1016/j.rse.2017.01.021>
- 870 Delworth, T., & Manabe, S. (1989). The Influence of Soil Wetness on Near-Surface Atmospheric Variability.  
871 *Journal of Climate*, *2*(12), 1447-1462. [https://doi.org/10.1175/1520-0442\(1989\)002<1447:TIOSWO>2.0.CO;2](https://doi.org/10.1175/1520-0442(1989)002<1447:TIOSWO>2.0.CO;2)
- 872 Dirmeyer, P. A. (2011). The terrestrial segment of soil moisture-climate coupling: SOIL MOISTURE-CLIMATE  
873 COUPLING. *Geophysical Research Letters*, *38*(16), n/a-n/a. <https://doi.org/10.1029/2011GL048268>
- 874 Dorigo, W. A., Wagner, W., Hohensinn, R., Hahn, S., Paulik, C., Xaver, A., Gruber, A., Drusch, M., Mecklenburg,  
875 S., van Oevelen, P., Robock, A., & Jackson, T. (2011). The International Soil Moisture Network: a data  
876 hosting facility for global in situ soil moisture measurements. *Hydrology and Earth System Sciences*, *15*(5),  
877 1675-1698. <https://doi.org/https://doi.org/10.5194/hess-15-1675-2011>
- 878 Entekhabi, D., Njoku, E. G., O'Neill, P. E., Kellogg, K. H., Crow, W. T., Edelstein, W. N., Entin, J. K., Goodman,  
879 S. D., Jackson, T. J., Johnson, J., Kimball, J., Piepmeier, J. R., Koster, R. D., Martin, N., McDonald, K. C.,  
880 Moghaddam, M., Moran, S., Reichle, R., Shi, J. C., & Van Zyl, J. (2010). The Soil Moisture Active Passive  
881 (SMAP) Mission. *Proceedings of the IEEE*, *98*(5), 704-716.  
882 <https://doi.org/https://doi.org/10.1109/JPROC.2010.2043918>
- 883 Findell, K. L., Gentine, P., Lintner, B. R., & Kerr, C. (2011). Probability of afternoon precipitation in eastern United  
884 States and Mexico enhanced by high evaporation. *Nature Geoscience*, *4*(7), 434-439.  
885 <https://doi.org/https://doi.org/10.1038/ngeo1174>
- 886 Gerke, H. H., & van Genuchten, M. T. (1993a). A dual-porosity model for simulating the preferential movement of  
887 water and solutes in structured porous media. *Water Resources Research*, *29*(2), 305-319.  
888 <https://doi.org/10.1029/92wr02339>
- 889 Gerke, H. H., & van Genuchten, M. T. (1993b). Evaluation of a first-order water transfer term for variably saturated  
890 dual-porosity flow models. *Water Resources Research*, *29*(4), 1225-1238.  
891 <https://doi.org/10.1029/92wr02467>
- 892 Gerke, H. H., & van Genuchten, M. T. (1996). Macroscopic representation of structural geometry for simulating  
893 water and solute movement in dual-porosity media. *Advances in Water Resources*, *19*(6), 343-357.  
894 [https://doi.org/10.1016/0309-1708\(96\)00012-7](https://doi.org/10.1016/0309-1708(96)00012-7)
- 895 Ghannam, K., Nakai, T., Paschalis, A., Oishi, C. A., Kotani, A., Igarashi, Y., Kumagai, T., & Katul, G. G. (2016).  
896 Persistence and memory timescales in root-zone soil moisture dynamics. *Water Resources Research*, *52*(2),  
897 1427-1445. <https://doi.org/https://doi.org/10.1002/2015WR017983>
- 898 Guo, Z., Dirmeyer, P. A., Hu, Z. Z., Gao, X., & Zhao, M. (2006). Evaluation of the Second Global Soil Wetness  
899 Project soil moisture simulations: 2. Sensitivity to external meteorological forcing. *Journal of Geophysical  
900 Research: Atmospheres*, *111*(D22), 2006JD007845. <https://doi.org/10.1029/2006JD007845>
- 901 Guo, Z., Dirmeyer, P. A., Hu, Z. Z., Gao, X., & Zhao, M. (2006). Evaluation of the Second Global Soil Wetness  
902 Project soil moisture simulations: 2. Sensitivity to external meteorological forcing. *Journal of Geophysical  
903 Research: Atmospheres*, *111*(D22). <https://doi.org/https://doi.org/10.1029/2006JD007845>
- 904 He, Q., Lu, H., & Yang, K. (2023). Soil Moisture Memory of Land Surface Models Utilized in Major Reanalyses  
905 Differ Significantly From SMAP Observation. *Earth's Future*, *11*(4).  
906 <https://doi.org/https://doi.org/10.1029/2022EF003215>
- 907 Huffman, G. J., Bolvin, D. T., Braithwaite, D., Hsu, K.-L., Joyce, R. J., Kidd, C., Nelkin, E. J., Sorooshian, S.,  
908 Stocker, E. F., Tan, J., Wolff, D. B., & Xie, P. (2020). Integrated Multi-satellite Retrievals for the Global  
909

910 Precipitation Measurement (GPM) Mission (IMERG). In V. Levizzani, C. Kidd, D. B. Kirschbaum, C. D.  
911 Kummerow, K. Nakamura, & F. J. Turk (Eds.), *Satellite Precipitation Measurement: Volume 1* (pp. 343-  
912 353). Springer International Publishing. [https://doi.org/10.1007/978-3-030-24568-9\\_19](https://doi.org/10.1007/978-3-030-24568-9_19)

913 Jawad, M., Bhattacharya, B., Young, A., & van Andel, S. J. (2024). Evaluation of Near Real-Time Global  
914 Precipitation Measurement (GPM) Precipitation Products for Hydrological Modelling and Flood  
915 Inundation Mapping of Sparsely Gauged Large Transboundary Basins—A Case Study of the Brahmaputra  
916 Basin. *Remote Sensing*, 16(10). <https://doi.org/10.3390/rs16101756>

917 Ji, P., Yuan, X., & Jiao, Y. (2023). Synergistic Effects of High-Resolution Factors for Improving Soil Moisture  
918 Simulations Over China. *Water Resources Research*, 59(12). <https://doi.org/10.1029/2023wr035513>

919 Katul, G. G., Porporato, A., Daly, E., Oishi, A. C., Kim, H. S., Stoy, P. C., Juang, J. Y., & Siqueira, M. B. (2007).  
920 On the spectrum of soil moisture from hourly to interannual scales. *Water Resources Research*, 43(5),  
921 2006WR005356. <https://doi.org/10.1029/2006WR005356>

922 Koster, R. D., Dirmeyer, P. A., Guo, Z., Bonan, G., Chan, E., Cox, P., Gordon, C. T., Kanae, S., Kowalczyk, E.,  
923 Lawrence, D., Liu, P., Lu, C.-H., Malyshev, S., McAvaney, B., Mitchell, K., Mocko, D., Oki, T., Oleson,  
924 K., Pitman, A.,... Yamada, T. (2004). Regions of Strong Coupling Between Soil Moisture and Precipitation.  
925 *Science*, 305(5687), 1138-1140. <https://doi.org/10.1126/science.1100217>

926 Koster, R. D., Dirmeyer, P. A., Hahmann, A. N., Ijpehaar, R., Tyahla, L., Cox, P., & Suarez, M. J. (2002).  
927 Comparing the Degree of Land–Atmosphere Interaction in Four Atmospheric General Circulation Models.  
928 *Journal of Hydrometeorology*, 3(3), 363-375. [https://doi.org/10.1175/1525-  
929 7541\(2002\)003<0363:CTDOLA>2.0.CO;2](https://doi.org/10.1175/1525-7541(2002)003<0363:CTDOLA>2.0.CO;2)

930 Koster, R. D., Guo, Z., Yang, R., Dirmeyer, P. A., Mitchell, K., & Puma, M. J. (2009). On the Nature of Soil  
931 Moisture in Land Surface Models. *Journal of Climate*, 22(16), 4322-4335.  
932 <https://doi.org/10.1175/2009JCLI2832.1>

933 Koster, R. D., Mahanama, S. P. P., Livneh, B., Lettenmaier, D. P., & Reichle, R. H. (2010). Skill in streamflow  
934 forecasts derived from large-scale estimates of soil moisture and snow. *Nature Geoscience*, 3(9), 613-616.  
935 <https://doi.org/10.1038/ngeo944>

936 Koster, R. D., & P. Mahanama, S. P. (2012). Land Surface Controls on Hydroclimatic Means and Variability.  
937 *Journal of Hydrometeorology*, 13(5), 1604-1620. <https://doi.org/10.1175/JHM-D-12-050.1>

938 Koster, R. D., Reichle, R. H., & Mahanama, S. P. P. (2017). A Data-Driven Approach for Daily Real-Time  
939 Estimates and Forecasts of Near-Surface Soil Moisture. *Journal of Hydrometeorology*, 18(3), 837-843.  
940 <https://doi.org/10.1175/JHM-D-16-0285.1>

941 Koster, R. D., Schubert, S. D., & Suarez, M. J. (2009). Analyzing the Concurrence of Meteorological Droughts and  
942 Warm Periods, with Implications for the Determination of Evaporative Regime. *Journal of Climate*, 22(12),  
943 3331-3341. <https://doi.org/10.1175/2008JCLI2718.1>

944 Koster, R. D., & Suarez, M. J. (1999). A Simple Framework for Examining the Interannual Variability of Land  
945 Surface Moisture Fluxes. *Journal of Climate*, 12(7), 1911-1917. [https://doi.org/10.1175/1520-  
946 0442\(1999\)012<1911:ASFFET>2.0.CO;2](https://doi.org/10.1175/1520-0442(1999)012<1911:ASFFET>2.0.CO;2)

947 Koster, R. D., & Suarez, M. J. (2001). Soil Moisture Memory in Climate Models. *Journal of Hydrometeorology*,  
948 2(6), 558-570. [https://doi.org/10.1175/1525-7541\(2001\)002<0558:SMMICM>2.0.CO;2](https://doi.org/10.1175/1525-7541(2001)002<0558:SMMICM>2.0.CO;2)

949 Mao, Y., Crow, W. T., & Nijssen, B. (2020). A Unified Data-Driven Method to Derive Hydrologic Dynamics From  
950 Global SMAP Surface Soil Moisture and GPM Precipitation Data. *Water Resources Research*, 56(2),  
951 e2019WR024949. <https://doi.org/10.1029/2019WR024949>

952 McColl, K. A., Alemohammad, S. H., Akbar, R., Konings, A. G., Yueh, S., & Entekhabi, D. (2017). The global  
953 distribution and dynamics of surface soil moisture. *Nature Geoscience*, 10(2), 100-104.  
954 <https://doi.org/10.1038/ngeo2868>

955 McColl, K. A., He, Q., Lu, H., & Entekhabi, D. (2019). Short-Term and Long-Term Surface Soil Moisture Memory  
956 Time Scales Are Spatially Anticorrelated at Global Scales. *Journal of Hydrometeorology*, 20(6), 1165-  
957 1182. <https://doi.org/10.1175/JHM-D-18-0141.1>

958 McColl, K. A., Wang, W., Peng, B., Akbar, R., Short Gianotti, D. J., Lu, H., Pan, M., & Entekhabi, D. (2017).  
959 Global characterization of surface soil moisture drydowns. *Geophysical Research Letters*, 44(8), 3682-  
960 3690. <https://doi.org/10.1002/2017GL072819>

961 Mei, R., & Wang, G. (2012). Summer Land–Atmosphere Coupling Strength in the United States: Comparison  
962 among Observations, Reanalysis Data, and Numerical Models. *Journal of Hydrometeorology*, 13(3), 1010-  
963 1022. <https://doi.org/10.1175/JHM-D-11-075.1>

- 964 Moghisi, S. S., Yazdi, J., & Salehi Neyshabouri, S. A. A. (2024). Multivariate Analysis of Rainfall Spatial  
965 Distribution and Its Effect on Stormwater Magnitudes. *Journal of hydrologic Engineering*, 29(2),  
966 05024002. <https://doi.org/10.1061/JHYEFF.HEENG-5941>
- 967 Nakai, T., Katul, G. G., Kotani, A., Igarashi, Y., Ohta, T., Suzuki, M., & Kumagai, T. o. (2014). Radiative and  
968 precipitation controls on root zone soil moisture spectra. *Geophysical Research Letters*, 41(21), 7546-7554.  
969 <https://doi.org/10.1002/2014GL061745>
- 970 Niu, G., Fang, Y., Neto, A. A. M., Guo, B., Zhang, X.-Y., Farmani, M. A., Behrangi, A., & Zeng, X. (2024).  
971 Representing Preferential Flow through Variably-Saturated Soils with Surface Ponding in a Large-Scale  
972 Land Surface Model over the Conterminous US. <https://doi.org/10.22541/essoar.172286649.90332939/v1>
- 973 Niu, G.-Y., Yang, Z.-L., Mitchell, K. E., Chen, F., Ek, M. B., Barlage, M., Kumar, A., Manning, K., Niyogi, D.,  
974 Rosero, E., Tewari, M., & Xia, Y. (2011). The community Noah land surface model with  
975 multiparameterization options (Noah-MP): 1. Model description and evaluation with local-scale  
976 measurements. *Journal of Geophysical Research*, 116(D12), D12109.  
977 <https://doi.org/10.1029/2010JD015139>
- 978 Niu, G. Y., Fang, Y. H., Chang, L. L., Jin, J., Yuan, H., & Zeng, X. (2020). Enhancing the Noah-MP Ecosystem  
979 Response to Droughts With an Explicit Representation of Plant Water Storage Supplied by Dynamic Root  
980 Water Uptake. *Journal of Advances in Modeling Earth Systems*, 12(11).  
981 <https://doi.org/10.1029/2020ms002062>
- 982 Oleson, K., Lawrence, D., Bonan, G., Flanner, M., Kluzek, E., Lawrence, P., Levis, S., Swenson, S., Thornton, P.,  
983 Dai, A., Decker, M., Dickinson, R., Feddema, J., Heald, C., Hoffman, F., Lamarque, J.-F., Mahowald, N.,  
984 Niu, G.-Y., Qian, T.,...Zeng, X. (2010). *Technical Description of version 4.0 of the Community Land  
985 Model (CLM)*.
- 986 Pastorello, G., Trotta, C., Canfora, E., Chu, H., Christianson, D., Cheah, Y.-W., Poindexter, C., Chen, J.,  
987 Elbashandy, A., Humphrey, M., Isaac, P., Polidori, D., Reichstein, M., Ribeca, A., Van Ingen, C.,  
988 Vuichard, N., Zhang, L., Amiro, B., Ammann, C.,...Papale, D. (2020). The FLUXNET2015 dataset and the  
989 ONEFlux processing pipeline for eddy covariance data. *Scientific Data*, 7(1), 225.  
990 <https://doi.org/10.1038/s41597-020-0534-3>
- 991 Poggio, L., de Sousa, L. M., Batjes, N. H., Heuvelink, G. B. M., Kempen, B., Ribeiro, E., & Rossiter, D. (2021).  
992 SoilGrids 2.0: producing soil information for the globe with quantified spatial uncertainty. *Soil*, 7(1), 217-  
993 240. <https://doi.org/10.5194/soil-7-217-2021>
- 994 Seneviratne, S. I., & Koster, R. D. (2012). A Revised Framework for Analyzing Soil Moisture Memory in Climate  
995 Data: Derivation and Interpretation. *Journal of Hydrometeorology*, 13(1), 404-412.  
996 <https://doi.org/10.1175/JHM-D-11-044.1>
- 997 Seneviratne, S. I., Koster, R. D., Guo, Z., Dirmeyer, P. A., Kowalczyk, E., Lawrence, D., Liu, P., Mocko, D., Lu, C.-  
998 H., Oleson, K. W., & Verseghy, D. (2006). Soil Moisture Memory in AGCM Simulations: Analysis of  
999 Global Land–Atmosphere Coupling Experiment (GLACE) Data. *Journal of Hydrometeorology*, 7(5), 1090-  
1000 1112. <https://doi.org/10.1175/JHM533.1>
- 1001 Seneviratne, S. I., Lüthi, D., Litschi, M., & Schär, C. (2006). Land–atmosphere coupling and climate change in  
1002 Europe. *Nature*, 443(7108), 205-209. <https://doi.org/10.1038/nature05095>
- 1003 Shellito, P. J., Small, E. E., Colliander, A., Bindlish, R., Cosh, M. H., Berg, A. A., Bosch, D. D., Caldwell, T. G.,  
1004 Goodrich, D. C., McNairn, H., Prueger, J. H., Starks, P. J., Van Der Velde, R., & Walker, J. P. (2016).  
1005 SMAP soil moisture drying more rapid than observed in situ following rainfall events. *Geophysical  
1006 Research Letters*, 43(15), 8068-8075. <https://doi.org/10.1002/2016GL069946>
- 1007 Shellito, P. J., Small, E. E., & Livneh, B. (2018). Controls on surface soil drying rates observed by SMAP and  
1008 simulated by the Noah land surface model. *Hydrology and Earth System Sciences*, 22(3), 1649-1663.  
1009 <https://doi.org/10.5194/hess-22-1649-2018>
- 1010 Šimůnek, J., & Van Genuchten, M. T. (2008). Modeling Nonequilibrium Flow and Transport Processes Using  
1011 HYDRUS. *Vadose Zone Journal*, 7(2), 782-797. <https://doi.org/10.2136/vzj2007.0074>
- 1012 Sourì, J., OmidvarMohammadi, H., Neyshabouri, S. A. A. S., Chooplou, C. A., Kahrizi, E., Akbari, H., Sourì, J.,  
1013 OmidvarMohammadi, H., Neyshabouri, S. A. A. S., Chooplou, C. A., Kahrizi, E., & Akbari, H. (2024).  
1014 Numerical simulation of aeration impact on the performance of a-type rectangular and trapezoidal piano  
1015 key weirs. *Modeling Earth Systems and Environment* 2024 10:4, 10(4). [https://doi.org/10.1007/s40808-  
1016 024-02058-4](https://doi.org/10.1007/s40808-024-02058-4)
- 1017 Taylor, C. M., Birch, C. E., Parker, D. J., Dixon, N., Guichard, F., Nikulin, G., & Lister, G. M. S. (2013). Modeling  
1018 soil moisture-precipitation feedback in the Sahel: Importance of spatial scale versus convective

1019 parameterization. *Geophysical Research Letters*, 40(23), 6213-6218.  
1020 <https://doi.org/10.1002/2013GL058511>

1021 Tuttle, S., & Salvucci, G. (2016). Empirical evidence of contrasting soil moisture–precipitation feedbacks across the  
1022 United States. *Science*, 352(6287), 825-828. <https://doi.org/10.1126/science.aaa7185>

1023 Xia, Y., Mitchell, K., Ek, M., Sheffield, J., Cosgrove, B., Wood, E., Luo, L., Alonge, C., Wei, H., Meng, J., Livneh,  
1024 B., Lettenmaier, D., Koren, V., Duan, Q., Mo, K., Fan, Y., & Mocko, D. (2012). Continental-scale water  
1025 and energy flux analysis and validation for the North American Land Data Assimilation System project  
1026 phase 2 (NLDAS-2): 1. Intercomparison and application of model products. *Journal of Geophysical  
1027 Research: Atmospheres*, 117(D3). <https://doi.org/10.1029/2011jd016048>

1028 Yang, K., Chen, Y., He, J., Zhao, L., Lu, H., Qin, J., Zheng, D., & Li, X. (2020). Development of a daily soil  
1029 moisture product for the period of 2002–2011 in Chinese mainland. *Science China Earth Sciences*, 63(8),  
1030 1113-1125. <https://doi.org/10.1007/s11430-019-9588-5>

1031 Yang, Z.-L., Niu, G.-Y., Mitchell, K. E., Chen, F., Ek, M. B., Barlage, M., Longuevergne, L., Manning, K., Niyogi,  
1032 D., Tewari, M., & Xia, Y. (2011). The community Noah land surface model with multiparameterization  
1033 options (Noah-MP): 2. Evaluation over global river basins. *Journal of Geophysical Research*, 116(D12),  
1034 D12110. <https://doi.org/10.1029/2010JD015140>

1035 Yousefi Sohi, H., Farmani, M. A., & Behrangi, A. (2024). How do IMERG V07, IMERG V06, and ERA5  
1036 Precipitation Products Perform Over Snow-ice-free and Snow-ice-covered Surfaces at a Range of Near  
1037 Surface Temperatures? *ESS Open Archive*. <https://doi.org/10.22541/essoar.172675931.16404474/v1>

1038 Yousefi Sohi, H., Zahraie, B., Dolatabadi, N., & Zebarjadian, F. (2024). Application of VIC-WUR model for  
1039 assessing the spatiotemporal distribution of water availability in anthropogenically-impacted basins.  
1040 *Journal of Hydrology*, 637. <https://doi.org/10.1016/j.jhydrol.2024.131365>

1041 Zebarjadian, F., Dolatabadi, N., Zahraie, B., Yousefi Sohi, H., & Zandi, O. (2024). Triple coupling random forest  
1042 approach for bias correction of ensemble precipitation data derived from Earth system models for  
1043 Divandareh-Bijar Basin (Western Iran). *International Journal of Climatology*, 44(7), 2363-2390.  
1044 <https://doi.org/10.1002/joc.8458>

1045 Zeng, X., Liu, J., Ma, Z., Song, S., Xi, C., & Wang, H. (2010). Study on the effects of land surface heterogeneities  
1046 in temperature and moisture on annual scale regional climate simulation. *Advances in Atmospheric  
1047 Sciences*, 27(1), 151-163. <https://doi.org/10.1007/s00376-009-8117-4>

1048 Zhang, X., Niu, G.-Y., Elshall, A. S., Ye, M., Barron-Gafford, G. A., & Pavao-Zuckerman, M. (2014). Assessing  
1049 five evolving microbial enzyme models against field measurements from a semiarid savannah-What are the  
1050 mechanisms of soil respiration pulses? *Geophysical Research Letters*, 41(18), 6428-6434.  
1051 <https://doi.org/10.1002/2014gl061399>

1052  
1053